STUDYING FUNCTIONAL MAGNETIC RESONANCE IMAGING WITH ARTIFICIAL IMAGING OBJECTS

Doctoral Dissertation

Ville Renvall

Aalto University
School of Science and Technology
Low Temperature Laboratory
Brain Research Unit

STUDYING FUNCTIONAL MAGNETIC RESONANCE IMAGING WITH ARTIFICIAL IMAGING OBJECTS

Doctoral Dissertation

Ville Renvall

Doctoral dissertation for the degree of Doctor of Science in Technology to be presented with due permission of the Faculty of Information and Natural Sciences for public examination and debate in Auditorium TU2 at the Aalto University School of Science and Technology (Espoo, Finland) on the 24th of March 2010 at 12 noon.

Aalto University
School of Science and Technology
Low Temperature Laboratory
Brain Research Unit

Aalto-yliopisto
Teknillinen korkeakoulu
Kylmälaboratorio
Aivotutkimusyksikkö

Aalto University
School of Science and Technology
Faculty of Information and Natural Sciences
Department of Biomedical Engineering and Computational Science

Aalto-yliopisto
Teknillinen korkeakoulu
Informaatio- ja luonnontieteiden tiedekunta
Lääketieteellisen tekniikan ja laskennallisen tieteen laitos

ABSTRACT OF DOCTORAL DISSERTATION	AALTO UNIVERSITY SCHOOL OF SCIENCE AND TECHNOLOGY P.O. BOX 11000, FI-00076 AALTO http://www.aalto.fi

Author Ville Renvall

Name of the dissertation
Studying functional magnetic resonance imaging with artificial imaging objects

Manuscript submitted 19.1.2010	Manuscript revised 9.3.2010

Date of the defence   24.3.2010

☐ Monograph	☒ Article dissertation (summary + original articles)

Faculty	Faculty of Information and Natural Sciences
Department	Department of Biomedical Engineering and Computational Science
Field of research	engineering physics, biomedical engineering
Opponent(s)	Professor Bruce R. Rosen
Supervisor	Professor Risto Ilmoniemi
Instructor	Academy Professor Riitta Hari

Abstract

Blood oxygenation level dependent (BOLD) functional magnetic resonance imaging (fMRI) is an indirect method for measuring information processing in the brain. The method has enabled mapping human brain function in an unprecedented variety of tasks and conditions, and with a spatial resolution of the order of 1 mm.

In this dissertation, artificial imaging objects, or phantoms, with adjustable signal intensity were used to simulate and investigate the generation of fMRI signals. The objective was to characterise, and devise means to characterise, fMRI signal components that arise from methodological reasons, impeding the correct physiological interpretation of the signals.

The first study involved building an fMRI phantom, where an electric current was applied to introduce magnetic field inhomogeneity within a magnetic resonance signal source. It was shown that the changes of field homogeneity and thus fMRI signal, largely corresponded to the human BOLD changes, even though the physical mechanisms were different.

The mechanical properties of phantoms and brain however differ. Thus it was important to look into the attributes of phantoms that would make the fMRI signal from the phantom similar to brain scanning data. The second study examined geometric distortions in the echo-planar imaging method—commonly employed in both fMRI and diffusion tensor imaging—using a purpose-built structural phantom. In the third study, another fMRI activation phantom was built. There the induction wires were located outside the source of the fMRI signal, and thus the partial volume effect limiting the usability of the first fMRI phantom was abated. The phantom was applied to induce artificial activations that could be utilized to deduce periods when simultaneously measured brain activations would yield deviant activation levels due to unphysiological causes.

In the last study, an fMRI phantom was used to show that transient fMRI signal components, often witnessed in brain activation data, could occur in the absence of corresponding physiological signal, resulting from the sole signal change.

Keywords   functional magnetic resonance imaging, fMRI phantom, fMRI, BOLD, transient

Tekijä   Ville Renvall

Väitöskirjan nimi
Toiminnallisen magneettikuvauksen tutkiminen keinokuvauskappaleiden avulla

Käsikirjoituksen päivämäärä 19.1.2010	Korjatun käsikirjoituksen päivämäärä 9.3.2010

Väitöstilaisuuden ajankohta   24.3.2010

☐ Monografia	☒ Yhdistelmäväitöskirja (yhteenveto + erillisartikkelit)

Tiedekunta   Informaatio- ja luonnontieteiden tiedekunta
Laitos   Lääketieteellisen tekniikan ja laskennallisen tieteen laitos
Tutkimusala   teknillinen fysiikka, lääketieteellinen tekniikka
Vastaväittäjä(t)   Professori Bruce R. Rosen
Työn valvoja   Professori Risto Ilmoniemi
Työn ohjaaja   Akatemiaprofessori Riitta Hari

Tiivistelmä

Toiminnallisella magneettikuvauksella (fMRI) voidaan mitata aivojen informaationkäsittelyä heijastava hemodynaaminen aivovaste pään ulkopuolelta. Menetelmällä on pystytty kartoittamaan aivotoimintaa ennennäkemättömässä laajuudessa jopa millimetrien paikkatarkkuudella.

Tässä työssä tutkittiin fMRI-signaaleja mallilaitteistoilla, joissa keinokuvauskappaleesta (fantomista) mitattavan signaalin intensiteettiä muuttelemalla voitiin simuloida aivovasteita. Erityisen mielenkiinnon kohteina olivat muista kuin fysiologisista tapahtumista johtuvat signaalimuutokset, jotka vaikeuttavat varsinaiseen aivotoimintaan liittyvien signaalien tarkkaa mittausta ja tulkintaa.

Ensimmäisessä osatyössä suunniteltiin ja rakennettiin fantomi, jonka fMRI-signaali muuttui kappaleen läpi kulkevan sähkövirran muuttuessa. Osoittautui, että sähkövirtaan liittyvät magneettikentän homogeniamuutokset vastasivat monilta osin aivojen hemodynaamisen vasteen tuottamia fMRI-muutoksia, vaikka niiden syntymekanismi onkin erilainen.

Fantomien mekaaniset ominaisuudet eivät kuitenkaan vastaa aivoja, joten seuraavaksi tutkittiin minkälaisin edellytyksin fantomin synnyttämät "aktivaatiot" olisivat mahdollisimman samankaltaisia aivoaktivaatioiden kanssa. Toisessa osatyössä käsiteltiin magneettikentän sekä fMRI:ssä ja diffuusiotensorikuvauksessa käytettävän echo-planar kuvausmenetelmän aiheuttamia geometrisia vääristymiä tarkoitusta varten tehdyn fantomin avulla. Kolmannessa osatyössä parannettiin toiminnallisen fantomin ominaisuuksia mm. siirtämällä induktiokelat magneettikuvaussignaalilähteen ulkopuolelle, minkä vuoksi edellisen fantomimallin haittana ollut osatilavuusefekti hävisi. Sovelluksena tutkittiin kuinka keinotekoiset aktivaatiot pystyisivät osoittamaan aivoaktivaatioissa mahdollisesti esiintyviä fysiologisista syistä riippumattomia intensiteettipoikkeamia.

Viimeisessä osatyössä osoitettiin keinokuvauskappaleen avulla, että fMRI:ssä usein havaittavien lyhytaikaisten signaalikomponenttien amplitudi ei välttämättä kuvasta vastaavia muutoksia aivotoiminnassa, vaan että nämä transientit voivat syntyä kuvausmenetelmän seurauksena pelkästään siitä syystä, että signaali muuttuu.

Asiasanat   toiminnallinen magneettikuvaus, fMRI-fantomi, fMRI, BOLD, transientti

Academic dissertation

Studying functional magnetic resonance imaging with artificial imaging objects

Author

Ville Renvall
Brain Research Unit and Advanced Magnetic Imaging Centre, Low Temperature Laboratory
Aalto University School of Science and Technology

Supervisor

Professor Risto Ilmoniemi
Department of Biomedical Engineering and Computational Science
Aalto University School of Science and Technology

Instructor

Academy Professor Riitta Hari
Brain Research Unit, Low Temperature Laboratory
Aalto University School of Science and Technology

Preliminary examiners

Professor Peter A. Bandettini
Section of Functional Imaging Methods, Laboratory of Brain and Cognition
National Institute of Mental Health
United States of America

Docent Gösta Ehnholm
Philips Medical Systems MR Finland

Official opponent

Professor Bruce R. Rosen
Athinoula A. Martinos Center for Biomedical Imaging and Department of Radiology, Massachusettes General Hospital
Harvard Medical School
United States of America

Table of contents

List of publications

This thesis comprises a summary and four publications (P1–P4).

P1 **Renvall V**, Joensuu R, Hari R (2006): Functional phantom for fMRI: a feasibility study. *Magnetic Resonance Imaging* 24(3): 315–320.

P2 Mattila S, **Renvall V**, Hiltunen J, Kirven D, Sepponen R, Hari R, Tarkiainen A (2007): Phantom-based evaluation of geometric distortions in functional magnetic and diffusion tensor imaging. *Magnetic Resonance in Medicine* 57(4): 754–763.

P3 **Renvall V** (2009): Functional magnetic resonance imaging reference phantom. *Magnetic Resonance Imaging* 27(5): 701–708.

P4 **Renvall V**, Hari R (2009): Transients may occur in functional magnetic resonance imaging without physiological basis. *Proceedings of the National Academy of Sciences of the United States of America* 106(48): 20510–20514.

Contributions of the author

In P1, I was responsible for carrying out the experiments and analysing the data, as well as writing the paper with input from other co-authors; together with the co-authors I designed the experiments. In P2, I planned, implemented, and analysed a part of the experiments, and participated in running and analysing of the other experiments, including the preliminary investigations on phantom filling; I contributed actively to data interpretation as well as writing. As the sole author in P3, I executed all steps of the work. In P4, I made the original discovery and run all experiments and simulations; with the co-author I devised the control experiments, interpreted the results, and wrote the manuscript.

Abbreviations

BOLD   blood oxygenation level dependent

EPI   echo planar imaging

FID   free induction decay signal

fMRI   functional magnetic resonance imaging

FOV   field of view

FT   Fourier transform

FWHM   full width at half maximum

GRE   gradient recalled

HRF   haemodynamic response function

MR   magnetic resonance

MRI   magnetic resonance imaging

NMR   nuclear magnetic resonance

r.f.   radiofrequency

ROI   region of interest

SE   spin echo

TE   echo time

TR   repetition time

Symbols

$\mathbf{B}$, B	magnetic field
$\mathbf{B}_0$, B_0	static polarizing magnetic field of the MRI scanner
B_1	excitation magnetic field
B_z	component of magnetic field in the z-direction
ΔB_z	inhomogeneity of z-component of magnetic field
χ_{m}	magnetic volume susceptibility
$\mathbf{e}_z$	unit vector in z-direction
ΔE	energy difference between spin states
$fSNR$	functional signal to noise ratio
$\mathbf{G}$	gradient of the z-component of magnetic field
G_i	gradient of the z-component of magnetic field in the i-direction
γ	gyromagnetic ratio
$\hbar$	Planck's constant $\approx 1.055 \times 10^{-34}$ J·s
I	spin quantum number
i	imaginary unit or index
k	Boltzmann constant $\approx 1.381 \times 10^{-23}$ m^2·kg·s^{-2}·K^{-1}
$\mathbf{k}$	k-vector
k_x, k_y	k-space coordinates
$\mathbf{M}$	magnetisation
$\mathbf{M}_i$, M_i	magnetisation in the i-direction
m_{I}	magnetic quantum number
$\boldsymbol{\mu}$	nuclear magnetic moment
N	number of samples, counting operator
ω	angular velocity, angular frequency
R_1	longitudinal relaxation rate
R_2	transverse relaxation rate
R_2^*	effective transverse relaxation rate
R_2'	inhomogeneity contribution to transverse relaxation rate
$\mathbf{r}$	position vector

ρ	spin density
S	signal intensity
$\mathbf{S}$	spin (angular momentum)
σ	standard deviation
T	temperature
T_1	longitudinal relaxation time
T_2	transverse relaxation time
T_2^*	effective transverse relaxation time
t	time
θ	azimuth angle
x', y', z'	spatial coordinates parallel to the frequency encoding, phase encoding, and slice selection gradients, respectively
x, y	spatial coordinates
z	spatial coordinate in the direction of B_0

The International System of Units (SI) is used throughout.

1 Introduction

Brain scanning technologies help appropriate diagnostics and treatments of some of the most oppressive illnesses that impair the person's ability to think, sense, and act. Magnetic resonance imaging[1] (MRI) is perhaps the most versatile of those technologies, having provided a unique view to the brain in action, revolutionising our concepts of *brain function*, as well as deciphering a multitude of physical properties without changes in the equipment. Applications of MRI usually produce maps where anatomically constrained regions appear distinctly. This contrast can be *programmed* to reflect various features of or within tissues.

Functional magnetic resonance imaging (fMRI) comprises methods whereby brain function can be studied employing MRI. Since its debut in the early 1990s, fMRI has matured and become a common imaging tool, especially in basic research, to provide new information on human brain function, including sensory systems, memory, cognition, social interaction, and even conscious perception. Beyond neuroscience, fMRI experimentation combines ingredients of statistics, physiology, physics, engineering, signal processing, and psychology, to name a few.

A robust and the most commonly utilised MRI signal reflecting neuronal activity derives from blood oxygenation level dependent (BOLD) modulations of the magnetic field. Since oxygenated blood is more diamagnetic than oxygen-depleted blood, and because nutrition and oxygen are supplied locally in the activated brain region on demand and even in excess of demand, the BOLD signal becomes informative of changes and locations of brain activations.

Echo-planar imaging (EPI) is the predominant MRI technique used to unravel the BOLD signal. The ultra-fast EPI is capable of scanning a complete plane image in tens of milliseconds. It is, however, intrinsically prone to artefacts, including those of poor magnetic field homogeneity. Both the speed *and* the particular type of artefact-vulnerability serve the purpose of acquiring information on brain function, because

---

[1] Literature references are postponed to the sections following this Introduction.

speed is required to track function—it happens that the BOLD signal changes following brain activations can last from a few seconds upwards—and the alterations of magnetisation following blood oxygenation level variations transpire by the same mechanism as the common susceptibility artefacts.

As the BOLD signal variation results from varying external magnetic field via magnetisation of blood, modifying the field by other means in a model system may cause similar effects to the nuclear magnetisation that eventually is measured and gives the signal. Whereas changes of magnetic (volume) susceptibility (χ_m), and consequently magnetic field homogeneity, bring about the magnetic field changes in the brain, a model system can utilise, *e.g.* electromagnetic induction to alter magnetic field homogeneity and that way simulate the BOLD responses.

But why is it desirable to investigate fMRI signal in a system other than the brain? Pragmatic reasons include the unyielding patience and ability of a model system, a machine, to stay immobile while an investigator turns knobs to perfect the measurement setup, its placid temper guaranteeing (almost) identical state and structure day after day, and the constant availability of the imaging target. It would be valuable to have means to calibrate fMRI scanners or studies, preferably during every measurement session. When this work commenced, apparently such devices were not available, but when we finalised the first system, two prototype devices for basically the same purpose had been demonstrated, one about a month earlier and the other the previous year. Yet another, more fundamental reason is the circularity of developing methods to study a limitedly characterised system, and validating them only against the system itself.

In this dissertation I studied fMRI with artificial imaging objects (for specific goals of the present work, see Chapter 3: Objectives). A major share of the work was done on assessing features desirable for such a model system, a *phantom* in imaging language, to be able to examine issues specific to fMRI, without resorting to scanning brains. Developing appropriate phantoms, and gaining the skills and knowledge to devise purposeful phantoms for specific problems was the initial objective, because only that enables approaching applications. This study commenced from a test of feasibility of controllably time-variant MRI signal phantoms, continuing through further developments on such phantoms, and eventually to an application exploring some fundamental aspects of transient signal components in fMRI, and the consequent proposition of a mechanism that could explain some apparent deviation of previous experiments and theory.

First, a relatively brief review of MRI, fMRI, and methodology relevant to this study is presented in Chapter 2. In Chapter 3, the objectives of the dissertation are laid out. Chapter 4 gives a succinct review on employed materials and methods, and summarises the publications that in part constitute this dissertation. Finally in Chapter 5, outcomes of the studies are discussed, and concluding methodological considerations and future directions wrap up this thesis.

Finally, publications P1–P4, included as appendices to this general summary, contain most of the original findings of this dissertation. They disclose the individual research hypotheses, methods, experiments, and specific discussions.

2 Background

Molecules, the subject of study of nuclear magnetic resonance (NMR) and magnetic resonance imaging (MRI), are composed of atoms containing electrons and nuclei. Interactions of and among these constituents give the whole world its characteristics. Each individual atom is capable of receiving and emitting a variety of differently energised photons. In MRI, the rays observed are of feeble energy, arising from the hyperfine splitting of nuclear energy levels; the energy of a unit of NMR radiation is about a millionth of that of visible light. Sophisticated equipment is required to animate and detect the tiny NMR signals.

The following sections describe concisely the physical and technological framework of this thesis, followed by a brief review of some related physiological aspects.

Nuclear magnetic resonance

Already 64 years ago, Bloch, Hansen, and Packard (Bloch 1946; Bloch *et al.* 1946a,b) and independently Purcell, Torrey, and Pound (1946) discovered interactions occurring between nuclei and radio frequency fields in the presence of a strong external magnetic field. Bloch (1946) was able to derive expressions for the dynamic behaviour of nuclear magnetisation and show that the nuclear spins behave as through electromagnetic induction. Purcell *et al.* (1946) exposed the quantum nature of the nuclear spin resonance. Immediately upon their discovery, nuclear magnetic relaxation properties were used to explain details of the structure of matter.

Four years later in 1950, Erwin Hahn discovered that nuclear magnetic signal could be recalled by subsequent radio frequency (r.f.) pulses, after the initial signal was gone. Both the r.f. pulse technique, applied in Bloch's work too, and the discovery of the nuclear magnetic memory were crucial for the latter applications. Magnetic resonance imaging as we know it now would not exist without. The subsequent sections, up until the section of magnetic resonance imaging, are based on textbook material, mainly on Liang and Lauterbur (2000) and Levitt (2003).

All nuclei containing an odd number of protons or neutrons have a non-vanishing spin quantum number (I) in their ground states. They have an intrinsic angular momentum, or spin (**S**), which is related to the nuclear magnetic moment ($\boldsymbol{\mu}$) by

$$\boldsymbol{\mu} = \gamma \mathbf{S}, \tag{1}$$

where γ is the gyromagnetic ratio specific to the nuclear species. Particles with $I \neq 0$ are often referred to as "spins". The hydrogen nucleus ^{1}H, or the proton, is a special case of such nuclei, and contemporary MRI concentrates heavily on proton imaging, although other NMR-active isotopes are utilized as well. For a proton, $I = \frac{1}{2}$ and consequently two possible values exist for its magnetic quantum number, $m_I = -\frac{1}{2}$ and $\frac{1}{2}$; its $\gamma = 267.522 \times 10^6$ rad·s^{-1}·T^{-1}. In a non-zero magnetic field (**B**), the energies of these two states differ by ΔE, which makes the proton susceptible for energy exchange, corresponding to electromagnetic radiation at angular frequency (ω) according to the Larmor equation,

$$\omega = \gamma B. \tag{2}$$

At room temperature, in an external magnetic field, a large number of otherwise undisturbed protons polarise between the two quantum states according to the well-known Boltzmann distribution:

$$\frac{N(m_I = \frac{1}{2})}{N(m_I = -\frac{1}{2})} = \exp\left(\frac{\Delta E}{kT}\right), \tag{3}$$

where N is the counting operator, k is the Boltzmann constant, and T is the absolute temperature of the spin system. Noting that, as stated by Planck's law,

$$\Delta E = \hbar\omega, \tag{4}$$

where $\hbar$ is Planck's constant (divided by 2π), it follows from Eqs. 3 and 4 that at room temperature and 3 T there is about one excess ^{1}H spin in the low energy state for every 10^5 spins of a sample of water, meaning that both states are almost equally occupied. However, a sample of 10^{20} spins already contains a surplus of 10^{15} low-energy spins. This inequality can be harnessed to yield an NMR signal, which immediately shows why high γ, **B**, and total number of spins all elevate the obtainable signal.

Bloch (1946) found out that when a sample of spins is energised, the dynamic behaviour of the resulting magnetisation (**M**) can be described by the (Bloch) equation:

$$\frac{d\mathbf{M}}{dt} = \gamma \mathbf{M} \times \mathbf{B} + \frac{1}{T_1}(\mathbf{M}_0 - \mathbf{M}_z) - \frac{1}{T_2}(\mathbf{M}_x + \mathbf{M}_y), \tag{5}$$

where t, is time, $\mathbf{M}_0$ is thermal equilibrium magnetisation (Eq. 3), and $\mathbf{M}_x$, $\mathbf{M}_y$, and $\mathbf{M}_z$ are the components of magnetisations in x-, y-, and z-directions. $\mathbf{M}_z$ signifies the deviation from thermal equilibrium, and $\gamma \mathbf{M} \times \mathbf{B}$ can be identified as a precessional term, indicating that the magnetisation vector constantly traverses a circular path around $\mathbf{B}$ (if it is constant) at the Larmor frequency. $1/T_1 = R_1$ and $1/T_2 = R_2$ are sample-specific decay or relaxation rates of the nuclear spin population (where T_1 and T_2 are the corresponding relaxation times):

After the excitation of a sample, the acquired signal decays at the apparent transverse relaxation rate, R_2^*. While the R_2^*-dependent signal is the primary signal observed, it has no fundamental significance, whereas the proper transverse relaxation rate, R_2, tells about the spin–spin interactions occurring in the sample. The rates differ by a term quantifying magnetic field inhomogeneities, R_2';

$$R_2^* = R_2 + R_2'. \tag{6}$$

R_2' is not observed as a separate entity. The physical interpretation of transverse relaxation is the loss of phase coherence of the spins. When the spins in a certain part of the object are initially energised, they are coherent, *i.e.* they have gained directional "preference" in the transverse plane. As the neighbouring spins reside in, *e.g.* slightly different magnetic fields, their Larmor frequencies differ, whereby the resultant magnetisation vector starts to decay as the spins "point" to progressively more divergent directions. Eventually the phase coherence giving rise to transverse magnetisation disappears altogether. It is possible to recover the R_2'-part of the decayed signal with the method of spin echoes (Hahn 1950), which effectively recovers the phase coherence after a delay.

A major contribution to R_2^* is due to magnetic susceptibility, which quantifies the magnetisability of materials. In biological systems the variations of χ_m are small, *e.g.* the difference of completely oxygen depleted and fully oxygenated red blood cells is $4 \cdot \pi \cdot 0.264 \times 10^{-6}$ (Spees *et al.* 2001), which gives rise to a difference of 10 µT in a 3-T external field.

R_1 is called the longitudinal, or spin–lattice relaxation rate, which specifies the sample's rate of return to the thermal equilibrium occupancy of m_I states after

excitation, or equivalently, the average duration the sample's constituents retain the excess energy. For all MRI purposes, $R_1 < R_2 < R_2^*$.

NMR experiment

In a typical pulsed NMR experiment, a sample is placed in or near a coil, which resides within a strong magnetic field (B_0), commonly from several up to about 20 T. The coil is used as an antenna to emit radiation at the (Larmor) frequency the sample can absorb and re-emit in a direction perpendicular to *z*-direction that is defined by B_0, *i.e.* $\mathbf{e}_z = \mathbf{B}_0/|\mathbf{B}_0|$. This perpendicular excitation field is called the B_1-field. After the alternating current in the coil has been switched off, a similarly alternating and typically exponentially decaying voltage, referred to as the free induction decay signal (FID), can be measured from the receive coil(s) (that can be the same as the transmit coil). NMR signal corresponds to the transverse nuclear magnetization of the sample

$$S(t) \propto \int_{\text{sample}} M_{xy}(\mathbf{r}, t) d\mathbf{r}, \tag{7}$$

where S is the signal, $\mathbf{r}$ is a position vector,

$$M_{xy}(\mathbf{r}, t) = M_{xy}(\mathbf{r}, 0)e^{-t/\text{T}_2}e^{-i\omega(\mathbf{r},t)t}, \tag{8}$$

and $M_{xy}(\mathbf{r}, 0)$ is the initial magnetisation.

If Eq. 8 is regarded in a frame of reference rotating at the angular frequency ω, then in these rotating coordinates, the term $e^{-i\omega t}$ can be dropped from the expression, and the relaxation term can be considered quite conveniently when $\mathbf{B}$ is constant and homogeneous. On the other hand, if $\mathbf{B}$ (or B_0) is inconstant or inhomogeneous, the phases of spins located at different $\mathbf{r}$ vary as well, which gives rise to R_2', and eventually, in rotating frame, the magnetic field can (approximately) be expressed as,

$$M_{xy}(t) = M_{xy}(0)e^{-t/\text{T}_2^*}. \tag{9}$$

Further, as a specific example, if B_0 at two locations differs by $4 \cdot \pi \cdot 0.264 \times 10^{-6}$, *e.g.* after 1 ms, the phases of the spins at those locations have accrued a phase difference of 27 radians (that can be rewound by the spin echo technique).

Magnetic resonance imaging

In 1973, Paul Lauterbur presented a methodology whereby the spatial distributions of signal sources could be distinguished at a greater accuracy than the wavelength of the

radiation involved in the effect (Lauterbur 1973). The methodology, then named zeugmatography, was applied to produce spatial maps of NMR signals, effectively beginning what would be known as MRI.

The next section describes the equipment (scanner) used in MRI. The subsequent sections concentrate on the use of that equipment. Textbooks by Liang and Lauterbur (2000), Levitt (2003), and Bernstein *et al.* (2004) have mainly been used as references.

Hardware

The core components of an MRI scanner are the three different magnets: the main magnet, the r.f., and the gradient systems.

The main magnet provides the static magnetic field B_0. Modern scanners employ superconducting electromagnets to produce the main field to create as large a population difference as possible between the spin energy levels. A high B_0 affects also the fMRI capabilities, apart from the maximum signal claimable from a sample, as will be discussed later. Currently, typical magnetic fields range from 1.5 to 7 T, and even higher in magnets used for human fMRI.

Not only high strength but also excellent homogeneity of the main magnetic field is necessary for an MRI magnet, as is evident from Eqs. 6–8. Therefore, the magnet is "shimmed" (historically with iron "shims", more recently using "shim coils") to compensate for any inhomogeneities. The permanent shimming provides the magnet good overall homogeneity, but usually the field is further homogenised separately for each subject under study. As a side note, the imaging sequence may contain additional field homogenisation or shim compensation to counter the remaining inhomogeneities, to allow investigation of certain highly inhomogeneous targets (Glover 1999a; Truong and Song 2008), or to correct for varying homogeneity resulting from, *e.g.* head motion (Morrell and Spielman 1997; Ward *et al.* 2002). Notwithstanding the individual shimming, the operator of the scanner has no control over the main magnet.

The r.f. system generates the resonance excitation fields and is also used for signal reception. It consists of three main parts, the transmitter, the receiver, and the coil. While coils are of high importance in MRI, their properties play little role in this work and thus will not be discussed further.

In normal (f)MRI use, the r.f. transmitter is tuned to the proximity of the Larmor frequency of protons at the B_0 of the scanner. The amplitude, the exact centre frequency of the r.f. field and its phase can be controlled.

The receiver is used to amplify, demodulate, and digitise the signal emitted by the sample after excitation and detected by the coil. In the demodulation process, a technique called quadrature detection is used to capture the complete complex-valued signal, whereby the phase of the signal can be recovered in addition to the magnitude (Levitt 2003). The digitised signal is then sent to reconstruction by specialised hardware.

A gradient in MRI refers to a (linearly) varying z-component of $\mathbf{B}$ (B_z). An MRI scanner usually comprises three gradient systems, used mainly for spatial encoding, one for each physical rectangular coordinate x, y, and z, produced by electric current driven in double-saddle type (x and y), and Maxwell-type (z) coils wound around the cylindrical scanner bore aligned parallel to the z-direction (the actual coil geometries are found with numerical simulation by the manufacturer, a practical tool for the simulation is the Biot–Savart law). The gradients are denoted as $G_i = \partial B_z / \partial i$ for $i = x$, y, and z, or $\mathbf{G} = \nabla B_z = (\nabla \mathbf{B}) \cdot \mathbf{e}_z$.

The users control these magnets with the user interface of the magnet console, where they, instead of giving gradient or r.f. instructions, set pulse sequence parameters, which convert to magnetic field pulses through the pulse sequence software. Thus, even though the magnet has only so many "moving parts" (shim coils, amplitudes of the three orthogonal B_z-gradient fields, r.f.-field's amplitude, frequency, and phase, and the position of the bed), with the pulse sequence, the user can invoke an almost unlimited wealth of physical information of the sample. Whereas Eq. 9 presents a simplified expression for transverse magnetisation (proportional to signal) from the application of a single r.f. pulse, by application of further r.f. and gradient pulses the signal can be made sensitive to T_1, T_2, spin density, and diffusion in different proportions, as well as to many other parameters (Bernstein *et al.* 2004).

Figure 1 provides an illustration of an MRI measurement environment.
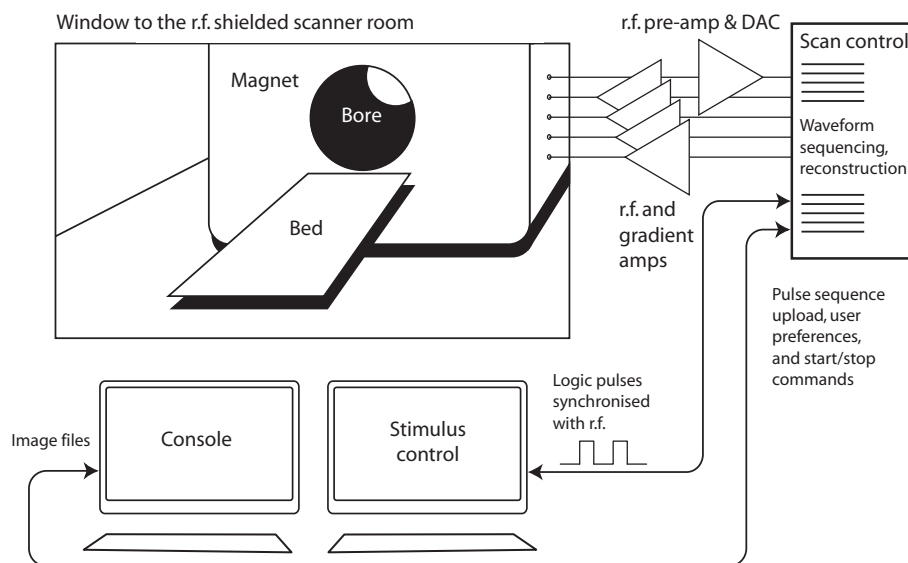
Figure 1: A schematic of fMRI measurement environment. The subject is resting on the bed with head inserted within or near a receive or transmit/receive radiofrequency head coil. The coil and the subject are both retracted in the magnet bore to the homogeneous B_0-field, to the isocentre of the applicable gradient fields. The user can determine the pulse sequences on the magnet console and send them to the computer operating the measurement hardware. The measurement results, *e.g.* images or spectra, are transferred back to the magnet console for operator's reference and storage. The scan control computer also informs the stimulus delivery system about every radiofrequency pulse in the pulse sequence software. Using that information, the stimuli can be accurately time-locked with the scan progress. Various stimulus systems can be controlled by a separate computer that in the present study was used to control the fMRI phantom.

Software

In modern MRI scanners, a special kind of software determines what instructions are given to the hardware producing, among other things, time-dependent magnetic fields, and when; *pulse-sequence-timing diagrams* summarise the key components of those instructions often revealing the idea of an imaging method at a glance. The pulse sequence determines the pulsed magnetic fields to produce the images but it also tells how the image is reconstructed from the measured data. Here, I call this software *pulse sequence software* whenever it is necessary to separate the software from the actual sequences of magnetic field pulses, called the *imaging sequence*. Whenever the distinction is immaterial, plain *pulse sequence* is used.

A pulse sequence normally contains a number of r.f. pulses—of definite powers, centre frequencies and amplitude modulation envelopes determining, for instance, the

bandwidths of the r.f. pulses—and the schedule of application of field gradients of certain amplitudes and durations. The pulse sequence software needs to make sure the play-out of all the magnetic fields is physically possible for the hardware, in practise within the manufacturer-determined limits, and it often also keeps track of remaining within safety limits of changing magnetic fields and absorbed r.f. energy.

Many pulse sequences can be split into two parts repeated in succession during a measurement. In the "r.f. module", the spins are energised, including preparatory r.f. pulses, such as those required to suppression of unwanted signal components arising from fat or protons outside the imaging volume; after proper preparation the signal can be acquired and digitised in the "readout module". Spatially selective spin-echo pulse is an example of r.f. module, whereas EPI exemplifies a readout module.

Often the coordinates assigned by the user do not coincide the physical scanner coordinates. As a unique advantage of MRI, the three gradient systems can be used together to scan any image orientation regardless of the geometry of the scanner. *E.g.*, a gradient tilted by 45° in the xy-plane can be achieved by applying an equal gradient amplitude in both directions. When the images are tilted this way, the physical coordinates are substituted by so-called logical set of coordinates, x', y', and z', conventionally matching, when applicable (see below), the frequency encoding, phase encoding, and slice selection directions, respectively; the pulse sequence software keeps track that calculations are done correctly. To avoid any confusion between different sides of the object, it is convenient, especially in fMRI where a lot of "homebuilt" software is used, and images are often too blurred to distinguish even gross anatomical landmarks, to include an MRI visible marker in the volume scanned.

To elucidate the discussion of image formation, in the following it is assumed that the sample studied is a perfectly homogeneous body of like nuclei so that each nucleus experiences an identical chemical environment. Also the B_0 field is assumed to be perfectly homogeneous. As a result, the Larmor frequency of each spin is the same.

Spatial encoding

Slice selection

Many MRI pulse sequences, including EPI (discussed in more detail later on) utilise an r.f. module, which excites the spins in a thin partition, a slice, whereby the signal can be considered as emanating from that volume only. Conceptually, slice selection can be accomplished by applying a magnetic field gradient perpendicular to the desired

slice, in z'-direction, and adjusting the excitation r.f. field to encompass the frequency band corresponding to the Larmor frequencies of the spins in the slice established by the gradient (Garroway *et al.* 1974). Information on the sample in its entirety can be obtained by appropriately modulating the r.f. band between successive measurements, thus looking at a "stack" of slices, one at a time. Fig. 2 illustrates a simple spatial encoding process.

More elaborate slice selection methods exist and are in routine use, such as spatial-spectral excitation (Block *et al.* 1997), which excites selectively only certain spectral species, *e.g.* either fat or water, within the determined partition.

Frequency encoding

The r.f. excitation (*e.g.* during slice selection) results in a narrow peak in the NMR spectrum. This spectral peak can be spatially encoded (Lauterbur 1973), *e.g.* so that the *frequency* of the signal depends on location. Superimposing an inhomogeneous, typically linear gradient, magnetic field on B_0-field (Lauterbur 1974) spreads the spectral peak across a wider frequency band, whereby the direction perpendicular to the gradient in x'-direction, ideally, forms isochromatic planes of spins during the acquisition of signal, or readout.

Phase encoding

Upon application of the r.f. field, quantum states of spins in the ensemble start to switch, from the low- to the high-energy state (excitation) as well as from the high- to the low-energy state (stimulated emission). The r.f. field rotates in phase with the nuclear magnetic moment precession, whereby—as the spins "see" a constant field—the newly excited spins produce a directional preference in the total spin population. In the rotating frame, these coherent spins give rise to a non-zero transverse magnetisation in a constant direction. In the laboratory coordinates, the directionality of the spin system is observed as an oscillating signal at the Larmor frequency, the FID.

14
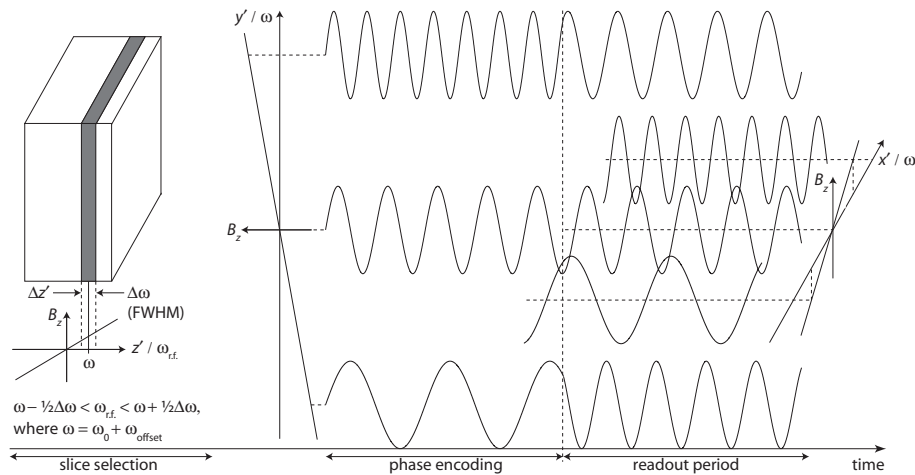
Figure 2: An illustration of an exemplary spatial encoding procedure. A partition of spins encompassing a frequency band $\Delta\omega$ (full width at half maximum of the slice profile) in the presence of field gradient $\partial B_z/\partial z'$ is first excited from the sample with an r.f. field of centre frequency (ω) offset from the mean Larmor frequency (ω_0) by ω_{offset}. After the excitation, and rewinding of phase errors due to the slice selection gradient (not shown), the spins are first phase encoded in presence of G_y'; after the period the spins at different locations on the y'-axis are at different phases when the readout period commences. During the readout, the x'-axis is frequency encoded, spins precess at different rates as a function of their position. The sequence is repeated for all prescribed slices and the k-space in the phase direction is filled by measuring each slice repeatedly with various G_y' amplitudes. For an example of a pulse-sequence-timing diagram, see Fig. 3. Note that in EPI, phase encoding is accomplished somewhat differently.

When a phase asymmetry has been established in the sample, in addition to frequency encoding, the signal can be phase-encoded with positional information (Kumar *et al.* 1975; Edelstein *et al.* 1980). Applying a magnetic field gradient between excitation and signal acquisition brings about phase discrepancy as a function of position along the direction of the gradient, the y'-direction, because the Larmor frequencies differ for the period. That is, integrating unequal angular velocities over a fixed period yields different final phases.

In most of the conventional pulse sequences, the frequency and phase encoding directions are perpendicular, and further, normal to the slice selection direction. "In-plane" refers to the plane spun by the frequency and phase encoded directions.

Now that signal is encoded with spatial information, a means is needed to decode it and produce an image. The so-called *k*-space formalism (Ljunggren 1983) enables reconstructing images in many circumstances where it would be very difficult to

otherwise determine how gradient waveforms affect the frequency and phase at each location, and how the thus obtained signal should be distributed in spatial coordinates. After arranging the data to the *k*-space, basically only a Fourier transform (FT) is required to reconstruct the image. Another advantage of the formalism comes from its easy interpretation in defining what and how should be sampled from the signal, in terms of gradient waveforms, to obtain an image of a specified detail level and field of view (Bernstein *et al.* 2004). The following paragraphs describe what this *k*-space is, and how the data can be arranged to it.

Spatial decoding

Any signal can be approximated by a linear combination of sine and cosine functions (or equivalently by complex exponential functions). Fourier transform is the systematic procedure yielding the amplitudes of these. If the signal is two-dimensional, *e.g.* a picture, the two-dimensional FT captures the contributions of each component function, often referred to as the (spatial) frequency components. Conversely, inverse FT of the frequency components yields the original signal. In fact, the *k*-space is just the (often) two-dimensional Fourier or frequency space.

Suitable arrangement of the NMR signal to the MRI *k*-space follows from the observation (Ljunggren 1983) that under the influence of field gradients, the signal in the rotating frame can be expressed as:

$$S(t) = \int \rho(\mathbf{r}) \exp\left(i\gamma \mathbf{r} \cdot \int_0^t \mathbf{G}(\tau)d\tau\right) d\mathbf{r}, \tag{10}$$

and that the FT of spin density $\rho(\mathbf{r})$ in space coordinate $\mathbf{r}$ is

$$\hat{\rho}(\mathbf{k}) = \int \rho(\mathbf{r}) e^{i\mathbf{k}\cdot\mathbf{r}} d\mathbf{r}, \tag{11}$$

above

$$\mathbf{k}(t) = \gamma \int_0^t \mathbf{G}(\tau)d\tau. \tag{12}$$

Thus, the signal expression is simplified to

$$S(t) = \hat{\rho}(\mathbf{k}(t)). \tag{13}$$

The above describes the signal in terms of the FT of the spin density in the variable $\mathbf{k}$. In the special case of two-dimensional gradient application, just the two components of $\mathbf{G}$ can be considered,

$$k_x(t) = \gamma \int_0^t G_x(\tau)d\tau, \text{ and}$$

$$(14)$$

$$k_y(t) = \gamma \int_0^t G_y(\tau)d\tau,$$

which defines the *k*-space coordinates (k_x, k_y). The temporal (measured) signal can thus be transformed to spatial information by viewing it as a linear combination of sinusoidal components with weights determined by the values of *k*-space.

Now, a pulse-sequence-timing diagram contains $G_x(t)$ and $G_y(t)$ (see Fig. 3 for an example, there G_{readout} and G_{phase} correspond to $G_x(t)$ and $G_y(t)$, respectively), and the trajectory in the plane of *k*-space can be traced. The play-out of the, say, x-gradient with positive amplitude moves the *k*-space trajectory to the positive k_x-direction. Negative y-gradient implies movement in the negative k_y-direction. If the *k*-space is sufficiently covered and sampled (Bernstein *et al.* 2004), $\rho(\mathbf{r})$, *i.e.* the spatial map of spin density, modified by additional factors accounting for relaxation, can be obtained by two-dimensional inverse Fourier transform. However, in the general case, when *k*-space is, *e.g.* not regularly sampled, the data have to be re-sampled before the transformation.

Echo-planar acquisition

Echo-planar imaging (EPI) (Mansfield 1977) sequence was the principal imaging "modality" in the experiments of P1–P4. Its main characteristics are now reviewed.

In echo-planar imaging, the *k*-space of each slice is filled by data acquired from (typically) a single r.f. pulse (resulting in an FID), or two pulses (spin echo). Spatial encoding of the in-plane directions varies slightly between different embodiments of EPI and in all instances the concept of phase encoding in EPI is somewhat different from most of other imaging methods. In EPI, phase encoding occurs practically (or literally) simultaneously with frequency encoding, *i.e.* signal acquisition.
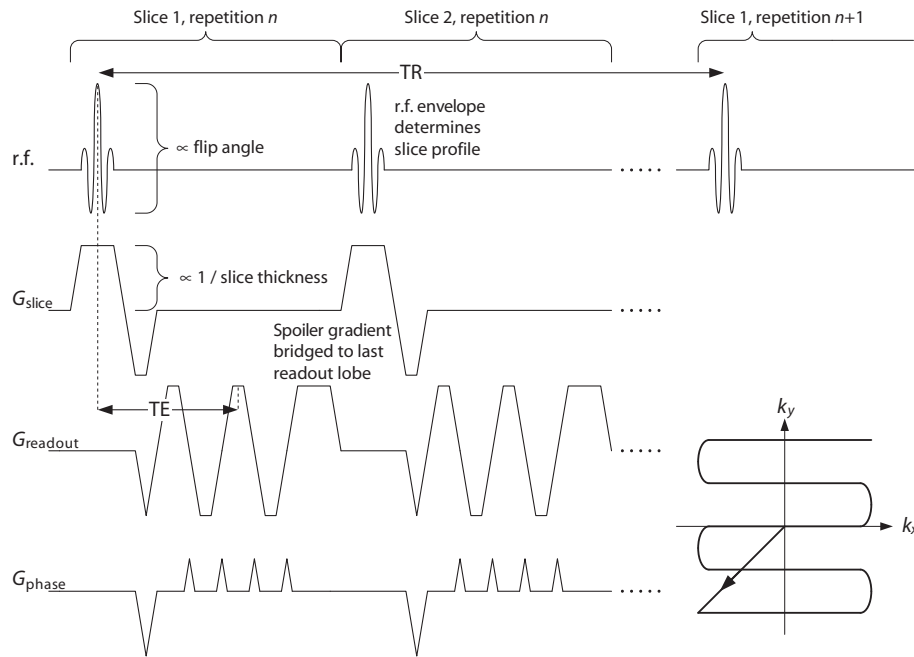
Figure 3: Pulse-sequence-timing diagram and k-space trajectory for Cartesian echo planar imaging of a stack of n images and 5 phase encodings per plane (in fMRI a minimum of 64 is normal). Different planes are selected by offsetting the frequency of the r.f. pulses played out in the presence of the slice selection gradient G_{slice}. In EPI, TR is defined as the time between successive excitations of a given slice. TE designates the time from the effective centre of the excitation pulse to the sampling of the centre of k-space. The actual TE of every phase encoding line is different from the others. The k-space trajectory traversed by the pulse sequence is shown. Pulse-sequence-timing diagram adapted from Bernstein *et al.* (2004).

The FID decays typically within tens of milliseconds, and therefore, to obtain a resolute image using the popular gradient-recalled (GRE) EPI, frequent sampling and strong gradients must be used to traverse and sample enough of the k-space. Alternatively, a sequence with multiple excitations per image plane, or by spin echo (SE) generation can be used to prolong the practical signal acquisition period; partial k-space sampling (Zaitsev *et al.* 2001) is possible as well. However, these strategies modify the contrast mechanism from the GRE EPI and in case of multiple excitations and SE, reduce the scanning efficiency, measured as image planes per time.

EPI is popular especially in applications where imaging speed is essential, including fMRI. The common Cartesian blipped EPI (Fig. 3) has become the standard in fMRI, and in addition to easy implementation and reconstruction, its artefacts are the easiest to interpret. However, of the alternatives, the spiral trajectory seems to be less prone to artefacts to begin with, while their interpretation might be difficult and requirements

for gradient precision are higher (Glover and Lee 1995; Block and Frahm 2005). Also, whereas spirals maintain the localisation of fMRI activations better in areas of high χ_m-induced gradients, the statistical significance of activations is higher with Cartesian EPI (Sangill *et al.* 2006). Thus the optimal choice of *k*-space traversal depends on whether the goal is sensitive detection or accurate mapping.

The pulse-sequence-timing diagram, shown in Fig. 3, illustrates schematically the implementation of the (Cartesian blipped) EPI sequence used in this work. It indicates various user selectable imaging parameters. The purpose of the following paragraphs is to briefly explain the basic imaging parameters.

EPI sequence parameters

Adjustments of imaging parameters can provide a wealth of physical information on the imaging samples. The information manifests as image contrast between different organs, healthy and lesioned (Damadian 1971; Damadian *et al.* 1974) tissue, *etc.*

Basic contrast-affecting variables are repetition time (TR), echo time (TE), and flip angle. In fMRI application of EPI, contrary to many other pulse sequences, TR denotes the time between successive excitations of a particular slice, meaning that during a TR the total imaging volume is scanned. A typical TR in fMRI ranges from hundreds of milliseconds to a few seconds. Sometimes TR can vary during the scan, *e.g.* when motion artefacts are reduced by synchronising the scanning with the heart rate of the subject (Guimares *et al.* 1998; Malinen *et al.* 2006). TE designates the time from (a specified instant of) the excitation pulse to the centre of the echo; in GRE EPI the sampling of the centre of the *k*-space, and in SE EPI the occurrence of the echo, which should coincide with the sampling of the centre of the *k*-space. Flip angle gives the nominal tilt of the bulk magnetization vector exerted by the excitation pulse, *i.e.* the amount of magnetisation excited. Flip angle often varies from the nominal value; most of all at the edges of the slice where it has to vary from 0 to the nominal value and (often) above. TR and TE in an EPI sequence are illustrated in Fig. 3.

Additionally, slice thickness, slice spacing or gap between slices, slice acquisition order, number of slices, slice orientation, size of the imaging matrix, field of view (FOV), and the directions of each method of spatial encoding are controllable by the user, among other things. The slice thickness is defined as the full width at half maximum (FWHM) of the bandwidth of an r.f. pulse, divided by the gradient amplitude. By specifying a gap between neighbouring slices, cross-talk between slices can be decreased (reduced overlap of the tails of the frequency spectra of the r.f. pulses

of adjacent slices) or more space covered in the slice-selection direction while ignoring the information in between. By interleaving the slice acquisition order, in contrast with sequential scanning, somewhat similar reduction in cross-talk can be achieved, yet the sample will be completely scanned. However, without a gap, the information content in adjacent slices will unavoidably be overlapping to some extent, defined by the slice profile and T_1. Size of the imaging matrix defines the pixel size of the image planes together with FOV, which is just another name for the in-plane extent of the image in cm.

Functional MRI

In typical fMRI experiments, subjects are receiving stimuli or performing tasks (or doing nothing), while their brain is scanned with an MRI technique sensitive to direct or indirect signs of neuronal activity. Statistically significant changes of the signal at certain volume elements (voxels) can be labelled as activation or deactivation.

A number of analysis methods, widely discussed in textbooks, *e.g.* in Huettel *et al.* (2004), have been utilised to find the network of brain areas associated with a task or a set of stimuli; popular methods include model-driven analyses, for instance the general linear model, which assigns weights to predictors that attempt to explain the total variance of the fMRI time series, and blind source separation, such as independent component analysis.

The temporal resolution of fMRI, determined by the sampling rate of successive imaging volumes, is much worse than of electrophysiological techniques, such as electro- and magnetoencephalography, but still adequate, and amenable to expansion by rather simple techniques, such as jittering the timing of stimulus presentation with respect to sequencing of the imaging repetition. However, as the effects measured with fMRI are also slow (seconds) as compared with electrical signalling of neurons (milliseconds), the temporal resolution of fMRI can be deemed sufficient.

Of the image acquisition methods yielding the data for analysis, GRE EPI results in T_2^*-weighted images (see Eq. 8), which are sensitive to field homogeneities, and thus to changes in blood oxygenation level. The GRE EPI images are also sensitive to confounding inflow effects, which can be remedied by dual-echo technique (Glover *et al.* 1996). Also different contrast mechanisms may be beneficial. SE EPI compensates for static inhomogeneity, leaving diffusion within the inhomogeneous field around red blood cells as the main mechanism for contrast, thus bringing the functional signal changes closer to neuronal tissue, because changes of signal can be detected from

veins and venules. The sensitivity of GRE EPI to the static inhomogeneity effect emphasises the contribution of the larger veins. Thus, SE activations occur slightly earlier (from tens to hundreds of ms) and co-localise better with neuronal activations than GRE activations (Hulvershorn *et al.* 2005). However, SE EPI has been noted to provide somewhat weaker functional signal than GRE EPI (approximately by a factor of two at 1.5 T (Bandettini *et al.* 1994). It has also been noted that not only T_2^* but T_2 too depend on the blood oxygenation (Thulborn *et al.* 1982), which is differently portrayed in SE and GRE.

Several other techniques can be applied to capture signs of brain function with MRI. Measuring cerebral blood volume using exogenous contrast agent (Belliveau *et al.* 1990; Belliveau *et al.* 1991), or non-invasively (Liu *et al.* 2000), diffusion imaging (Song *et al.* 1996; Le Bihan *et al.* 2006; Miller *et al.* 2007; Roberts *et al.* 2007; Aso *et al.* 2009), and perfusion imaging, *e.g.* by use of arterial spin labelling techniques (Wong *et al.* 1998) exemplify non-BOLD techniques. Voxel-based morphometry (Ashburner and Friston 2000), tractography, and other structural imaging methods, are also useful for understanding changes occurring in the brain. Detecting neuronal signals directly is currently below the sensitivity limit of MRI, although scattered evidence (Bodurka and Bandettini 2002) and simulations endorse the possibility (Park and Lee 2007; Cassará *et al.* 2009). However, other attempts to show such action *in vivo* have failed thus far (Parkes *et al.* 2007; Tang *et al.* 2008), whereas *in vitro*, neuronal electric activity has been detected with MRI (Petridou *et al.* 2006).

For now, however, blood oxygenation level dependent (BOLD) techniques (Ogawa *et al.* 1990; Bandettini *et al.* 1992; Kwong *et al.* 1992; Ogawa *et al.* 1992) are used in a vast majority of fMRI studies and, therefore, if not stated otherwise, plain fMRI typically refers to BOLD fMRI. In this work, fMRI indicates BOLD and BOLD-like signals (as simulated by phantoms).

All fMRI techniques suffer from relatively low functional signal-to-noise ratio,

$$fSNR = \frac{S_{\text{act}} - S_{\text{rest}}}{\sigma}, \tag{15}$$

where S_{act}, S_{rest}, and σ are the image intensities at a responding voxel during activation and rest, and the standard deviation of the image intensity in that voxel (*e.g.* at rest), respectively. Consequently, both spatial and temporal averaging are commonly used to increase $fSNR$.
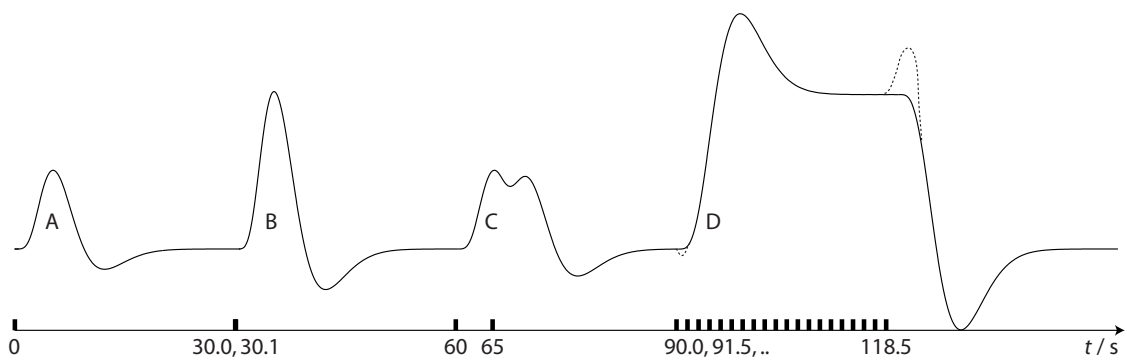
Figure 4: Time course of a hypothetical, noiseless fMRI experiment, where a brain area responds to stimulus impulses perfectly linearly. A single impulse (A) elicits a haemodynamic response characteristic of that area (the canonical HRF), two impulses (B) applied in quick succession (0.1 s separation) yield approximately the same response as a single stimulus, but with double amplitude (vertical direction indicates signal intensity). When the inter-stimulus interval increases to 5 s (C), the response spreads over a longer time period, and when several successive stimuli are given every 1.5 s (D), the typical shape of blocked-stimulus response arises. In (D), the dotted lines depict the "initial dip" and the post-stimulus overshoot (see text). The bars on the time-axis show the stimulation sequence.

Haemodynamic response function

A central concept in fMRI is the haemodynamic response function, HRF. Its importance in fMRI analysis stems from the theoretical proposition that knowing the HRF and stimulation pattern, the emerging fMRI signal can be evaluated by convolving the stimuli with the spatially varying yet fixed HRF. Conversely, from a full functional response of the brain, the activation pattern is statistically obtained using an HRF model (Lange and Zeger 1997). These properties assume that the haemodynamic response is a linear system, having the scaling property and obeying the principle of superposition.

To exemplify the superposition property in the current context, Fig. 4 illustrates the HRF to a single stimulus (A) as well as the linear prediction of the output of two successive stimuli of different inter-stimulus intervals (B and C). As a notion, the linearity considered here should actually be between neuronal activity and the HRF (Boynton *et al.* 1996), not between stimuli and HRF as is usually assumed. Linearity between stimuli and the HRF can still exist (Boynton *et al.* 1996), if the neural system can respond linearly to stimuli but, *e.g.* with short inter-stimulus intervals linearity does not generally hold (Huettel and McCarthy 2000; Huettel *et al.* 2004).

Lange and Zeger (1997) noticed that the main characteristics of fMRI signal following neuronal activity appear similar to a gamma function. Friston *et al.* (1998) developed a model to account for event-related fMRI responses, in which a second gamma-function was subtracted from the first to account for a post-stimulus undershoot. This doubly gamma-variate function has been subsequently referred to as the canonical HRF:

$$h(t) = \left(\frac{t}{d_1}\right)^{a_1} e^{-\frac{t-d_1}{b_1}} - c \left(\frac{t}{d_2}\right)^{a_2} e^{-\frac{t-d_2}{b_2}}. \tag{16}$$

Figure 4A illustrates the function with the parameter choices derived from auditory responses (Glover 1999b) with $a_1 = 6.0$, $a_2 = 12.0$, $b_1 = 0.9$ s, $b_2 = 0.9$ s, $c = 0.35$, and $d_i = a_i b_i$ are the times to the peaks.

Components of HRF

In a typical block-design fMRI experiment, where the stimuli are presented to the subjects in periods alternating with a rest or control condition, the BOLD response is often of similar periodic appearance, except that its shape contains transient components, much like the 30-s (simulated) stimulation illustrated in Fig. 4D, where a series of 20 impulses with 1.5-s inter-stimulus intervals has been convolved with the canonical HRF. As is evident in the figure, the haemodynamic response starts with a delay, followed by an increase of the fMRI signal that overshoots before reaching a plateau of sustained response. After the stimulus presentation, the signal decays and returns to a constant rest level through an undershoot. In addition, the initial rise of the signal is sometimes preceded by a transient signal decrease, the "initial dip", and at the end of stimulation, just before signal starts to decay, an occasional overshoot may be observed, as schematically indicated by the (hand-drawn) dotted lines in Fig. 4D.

The main contribution to the haemodynamic response in BOLD fMRI is quite universally accepted to result from the decreased fraction of deoxyhaemoglobin in the blood, resulting in a more homogeneous local magnetic field, thus yielding less dephasing of spins.

An exhaustive review on modelling the haemodynamic response summarised the experimental observations on the contributions to the HRF (Buxton *et al.* 2004). Of the different models, the Balloon model (Buxton *et al.* 1998) explains all the principal fMRI transients, the initial dip, the overshoot, as well as the undershoot in terms of blood volume, blood flow, and oxygen metabolism changes. Still, the cause, meaning,

and variability of fMRI transients remain debated, the post-stimulus undershoot seemingly most so.

Jones *et al.* (1998), likewise, investigated the undershoot and largely agreed with the Balloon model. Since then, more accurate views have been sought to explain the undershoot; the proposed mechanisms include lingering of passive ballooning (or expanding) of post-capillary vessels leading to increased venous blood volume (Mandeville *et al.* 1999; Mildner *et al.* 2001; Emir *et al.* 2008; Chen and Pike 2009; Tang *et al.* 2009) and prolonged oxidative metabolism (Jones 1999; Schroeter *et al.* 2006; Frahm *et al.* 2008). All the above studies supporting prolonged oxidative metabolism employed visual stimulation, in the ballooning group also other types of stimuli were used.

The transients in general seem to have different spatial distribution in the brain than the sustained responses, suggesting different underlying mechanisms (Chen *et al.* 1998; Seifritz *et al.* 2002; Fox *et al.* 2005a), and even different causes in different regions in the visual system (Harshbarger and Song 2008). The onset overshoot has been found to differ in control subjects and schizophrenia patients (Fox *et al.* 2005b). Neural activity patterns indistinguishable from the sustained BOLD response may be recovered from the post-stimulus undershoot (Sadaghiani *et al.* 2009).

Whereas the onset and post-stimulus *over*shoots have received only sporadic interest, the "initial dip", occasionally occurring within 2 s after stimulus presentation, has been much discussed in fMRI textbooks and reviews. The enthusiasm for the initial dip stems from mainly two factors: the initial dip is thought to be spatially—and, obviously, temporally—closer to the neuronal activity than the main BOLD response, and knowing its generation mechanism would answer questions about potential dynamic decoupling of cerebral blood flow and oxygen metabolism (Buxton 2001).

Shedding light to the early transients, a near-infrared study in cats and monkeys (Frostig *et al.* 1990) demonstrated that soon (200–400 ms) after the onset of neuronal activity, oxygen is delivered from the capillaries with high spatial precision, followed by an increase in blood volume 200–400 ms later (400–800 ms from the neuronal activity), and an increase in the amount of oxyhaemoglobin less than 1000 ms later. Qualitatively similar but slower early responses were reported in cats (Malonek and Grinvald 1996), laying foundation for the "initial dip" observed in fMRI. Afterwards, a large number of optical studies have both found and *not* found physiological basis for the initial dip, especially the dip is often absent in rodents both in optical studies

(Lindauer *et al.* 2001; Vanzetta and Grinvald 2001; Lindauer *et al.* 2002) and fMRI (Marota *et al.* 1999; Silva *et al.* 2000). While the majority of initial dip evidence comes from the visual system, in humans, the initial dip has also been found in the motor area (Yacoub and Hu 2001).

The initial dip has, thus, not been observed consistently, which impedes its interpretation. Table 1 collects data from papers dealing with the fMRI initial dip in healthy subjects and animals. Despite the variability across studies, some interesting patterns can be perceived from a strictly technical point of view. The first striking coincidence is the relatively short TR used in all experiments. As the initial dip in humans is at maximum typically ~2 s (range 1–3 s in the Table entries) after the stimulus presentation has begun, experiments with substantially longer TR could, in that regard, capture the signal. Moreover, studies jittering the stimulus timing with respect to scan sequencing should be sensitive to signal changes occurring at any phase of the stimulus presentation. Also, the studies with sagittal or coronal slices have yielded high percent signal changes of the initial dip. These observations will be processed further in the Discussion.

Of phantoms

In MRI, phantoms are used as imaging targets to verify and validate image quality, including signal level uniformity over time (Weisskoff 1996), to ascertain the proper functioning of the MRI device (McRobbie *et al.* 2005). As phantoms are, desirably, stable, significant changes in imaging conditions are often recognised as abnormalities in the images of phantoms acquired using a fixed set of imaging preferences. Such changes can indicate scanner problems or the presence of external noise sources, *e.g.* incompatible peripheral devices or movement of heavy machinery in the vicinity of the magnet installation (Durand *et al.* 2001). Many common problems with MRI scanners introduce characteristic patterns in images, some of which are apparent regardless of the object; others arise more subtly requiring a consistent quality assurance protocol for detection. For instance, gradual wearing of hardware components leads to deteriorating signal-to-noise ratio, and at some point, service is due, else diagnostic and scientific value of the imaging data will degenerate.

Table 1: Studies reporting the initial dip. B_0, TR, slice orientation, slice thickness (thi.), and percent signal change (ΔS / %) of fMRI signal during the initial tip are shown for each study (if information was provided).

B_0 / T	TR / ms	slice orient.[1]	thi. / mm	ΔS / %[2]	Reference
3	500	axial	4 and 8	−0.16 or −0.24	(Behzadi and Liu 2006)
4.7 and 9.4	500 or 2 × 250[2]		2	−1.5 (cat)	(Duong *et al.* 2000)
4	4 × 150[3] or 300	sagittal	5	−2.16 (max). or −1.61 (max.)	(Hu *et al.* 1997)
2	400	oblique along calcarine fissure	5	−0.27	(Janz *et al.* 2000)
4.7 and 9.4	500		2	−0.28 (cat)	(Kim *et al.* 2000)
4.7	4 or 8 segments 250 ms each		1 or 2	from −0.5 to −1 (monkey)	(Logothetis *et al.* 1999)
4	100	sagittal	5–8	−1	(Menon *et al.* 1995)
4	500	oblique along calcarine	3.75	"significant"[4]	(Roberts *et al.* 2007)
1.5	300	oblique along calcarine or sagittal	N/A	−0.42	(Yacoub and Hu 1999)
4	500	sagittal	5	−1.68 (max.)	(Yacoub *et al.* 1999)
7	400	sagittal	5	−0.75 (by ruler from a graph)	(Yacoub *et al.* 2000)
4	400	coronal	5	−1.172 (max.)	(Yacoub and Hu 2001)
7	300 or 450	sagittal	2	−0.85 (by ruler from a graph)	(Yacoub *et al.* 2001)
3	1000		3	−0.5	(Yeşilyurt *et al.* 2008)

[1]Of human studies, where available

[2]The signal change percentages were provided irregularly in the articles

[3]Multi-shot EPI

[4]No account on percent signal change was provided. It was noted in the study that the initial dip was statistically significant in loci where the positive BOLD response and diffusion-detected activation were co-localised. In such locations where the diffusion measure showed no activation, the initial dip was absent, giving further support for better localisation of the initial dip than the positive BOLD response.

The impact of different imaging options or sequences on image properties can be compared having a suitable phantom as the imaging object. Different finely structured phantoms can be used to study resolution (in different directions), slice profile, geometric distortions, *etc.*, as the spatial structure of the phantoms is known *a priori* to a high precision. Essential properties of different tissues in MRI (Bottomley *et al.* 1984; Spees *et al.* 2001) can obviously be best studied with phantoms of matching

qualities (Kato *et al.* 2005). Anthropomorphic phantoms are useful in studying and combating artefacts likely arising *in vivo* (Rice *et al.* 1998; Shmueli *et al.* 2007), because especially susceptibility artefacts are highly shape sensitive, and vary in different encoding directions (Lüdeke *et al.* 1985). Unstructured or more coarsely structured phantoms are typically used to examine signal and noise (bulk and distribution of), ghosting, and stability over longer scan periods, such as during fMRI.

Additional advantages of phantoms as compared with volunteer subjects include invariability over time, constant availability, and the fact that phantoms cause no physiology-related artefacts. However, many technical developments specifically target physiological signals or reduction of, *e.g.* movement artefacts; in these cases standard phantoms are of little use. A fundamental disadvantage is that the actual objects of interest are rarely phantoms, therefore the ultimate tests of new imaging methods, pulse sequences, parameters, or protocols need to be performed on volunteers, but often the processes can be expedited cost-effectively using phantoms.

Phantoms for EPI

EPI is intrinsically very susceptible to image imperfections, especially to direction-dependent distortion. EPI has a low bandwidth in the phase encoding direction, meaning that a change of Larmor frequency by only tens of Hz displaces the signal from a voxel to the neighbour. In addition to displacement, in the presence of magnetic field gradients, a voxel comes to contain a range of differently precessing nuclei, whereby the spins do not rephase at the centres of gradient echoes, resulting in signal void. Hence, a phantom for EPI demands that the constituents are magnetically highly similar, as quantified by χ_m.

fMRI phantoms

Normal phantoms are crucial in every fMRI laboratory and useful for collaborations between research facilities (Friedman and Glover 2006) because many aspects of acquisition, analysis, reproducibility, and post processing can be validated against such phantoms However, they do not provide the temporal variability to the signal that is the key ingredient of fMRI. Deterministic variation of physical parameters causing signal intensity modulation in a manner similar to that in the brain would yield in imaging results the full scope of features due to the imaging process. The total picture is harder to achieve by computational simulation, because *all* the features of the imaging system and object physics would need to be known and realised. The total picture is also hard to obtain by scanning real brains, because they cannot be

accurately controlled and are deterministic only to the extent of the physiology. In this dissertation, in three of the four studies (P1, P3, P4) phantoms with remotely adjustable signal (fMRI phantom) were used.

A number of fMRI phantoms and related devices have been developed. The fMRI phantoms presented by Joensuu *et al.* (2004) and Koopmans *et al.* (2004), and in P1, P3, and P4 used electric current to modulate magnetic field and thus signal acquired during fMRI experiments. Similar techniques have been adopted while striving to directly detect electric activity of brain using MRI (Bodurka *et al.* 1999; Bodurka and Bandettini 2002), more generally in magnetic resonance current density imaging (Scott *et al.* 1991), and also in a very practical application, to visualize catheters in MRI (Glowinski *et al.* 1997; Adam *et al.* 1998). In other fMRI phantom embodiments, the signal level was modulated by adjusting the tuning of a resonant circuit around an MRI signal source (Zhao *et al.* 2003; Cheng *et al.* 2004; Cheng *et al.* 2006), and by exchange of medium within the imaging volume during fMRI (Olsrud *et al.* 2008). The access to controllable signal variation can be used to reproduce virtually any temporal evolution of the signal, such as the canonical HRF, and this benefit has been used to correct for aliasing occurring in deconvolution of the hemodynamic response in event-related fMRI (Li *et al.* 2007).

Phantom construction

The fMRI phantoms consist of a minimum of four components: the vessel, signal delivery system, MRI-active medium (signal medium), and MRI-signal modulator.

The *vessel* is typically made of some plastic material; for example polymethyl methacrylate, *e.g.* Plexiglas® and Perspex®, is often appropriate because it is transparent and reasonably workable. Moreover, χ_m of polymethyl methalcrylate is close to water's: values -9.0×10^{-6} for Plexiglas (Thomas *et al.* 1993) *vs.* -9.05×10^{-6} for water (Schenck 1996), a biologically valid surrogate signal source. Polycarbonate would be easier to machine but it is magnetically further away from water. When prototyping or producing phantoms in small batches, the phantoms often need to be machined rather than moulded, and one needs to be meticulous about a clean working environment including new drill bits of "nonmagnetic" materials and overall careful handling.

In studies P1 and P3, the phantoms were to be small, to basically fit inside a head coil together with the subject's head. In phantoms of compact size, the edges of the vessel are necessarily close by the region of interest (ROI) of the signal medium, and thereby

not only the vessel material but also the air surrounding the phantom can cause susceptibility gradients. Sometimes it may be advantageous to match the susceptibility of the phantom and the signal medium with air (Davis 1998; Bakker and de Roos 2006) rather than water. An important detail of the vessel is its filling mechanism because the vessel should be kept full. The requirement can be to some extent circumvented by including a reservoir volume that does not need to be full.

The *signal delivery system* can be electric, fibre-optic, pneumatic, wireless, pre-programmed memory or other signal transferral pathway delivering the signal adjustment information to the MRI signal modulator. The signalling system must be MRI compliant of second kind, as termed by Schenck (1996), especially it must be non-magnetic, tolerant to electromagnetic disturbances, and must not generate electromagnetic disturbances visible in MRI. If the delivery system penetrates the r.f.-shield of the examination room, sufficient isolation must be implemented to reduce artefacts and protect equipment. It is worth pointing out that a device safe at, say, 3 T is not necessarily so at 1.5 T, mainly because of different wavelengths of the r.f. fields. The output performance requirements are dictated by the experiments to be carried out but at least stability and critical damping of step responses are useful properties.

The characteristics of the *signal medium* depend on the purpose of the phantom. Properties that must be considered, and can be modulated in a typical liquid or gel signal media, include chemical composition, relaxation times, electric conductivity and permittivity, viscosity, and χ_m.

Chemical composition affects the obtainable NMR spectrum, which in typical MRI phantoms should desirably be either very simple, *e.g.* a single water peak, or similar with a certain tissue. A simple spectrum is useful in investigating the proper functioning of the scanner, whereas a more natural spectrum would provide information about obtainable image quality *in vivo* and thereby help to optimise sequence parameters for brain scanning.

To receive anatomically valid information on the applicability of an imaging protocol using a phantom, the relaxation times of the signal medium should be in par with the tissues of interest. Particulars of producing solutions with a variety of different relaxation times (Schneiders 1988; Rice *et al.* 1998; Kato *et al.* 2005) and tissue relaxation times at different field strengths (Damadian *et al.* 1974; Bottomley *et al.* 1984; Henriksen *et al.* 1993; Wansapura *et al.* 1999; Spees *et al.* 2001; Lu *et al.* 2004;

Stanisz *et al.* 2005) are adequately available in the literature. For high magnetic fields, data are more sporadic (Shmueli *et al.* 2007).

The correct electric conductivities and permittivities in a phantom are important so that the r.f. field distributions would be similar than those that arise when humans are irradiated. Especially in high-field MRI, where the wavelength of the r.f. inside tissue is comparable to the tissue dimensions, and r.f. penetrates poorly to tissue because of its conductivity, the field distributions are irregular and concentrate near the surfaces. (Yang *et al.* 2004).

Viscosity affects the phantom's sensitivity to movements and vibration. For example, spatial encoding of an object containing low-viscosity liquid might fail as a result of bulk motion which takes a long while for stabilising. Furthermore, vibrations caused by the scanner, especially with pulse sequences requiring high gradient slew rates, such as in diffusion tensor imaging (Hiltunen *et al.* 2006), might keep low-viscosity medium in motion throughout the scanning. However, changing a solution's viscosity affects its T_1 relaxation process, in the neighbourhood of viscosity of liquid water, T_1 decreases with increasing viscosity (Bloembergen *et al.* 1947), which should be taken into account when otherwise tuning the relaxation parameters.

Since the material for the vessel must normally be chosen from a set of commonly available materials, of which information of some physical parameters, especially χ_m, is typically missing, a moderately appropriate material often has to suffice. Particularly, when the vessel must be compact, the susceptibility of nearby air (Davis 1998) must be compensated by modifying the χ_m of the signal medium, in order to obtain acceptable signal in EPI. For a magnetically dilute system, the susceptibility of a solution can be calculated from those of the solutes by Wiedemann's law of magnetic susceptibilities in magnetically dilute solutions (Mulay 1963). The χ_m-modulating substances can, however, affect the relaxation times. *E.g.*, Gd-based contrast agents increase χ_m and decrease T_1.

All the abovementioned signal medium properties depend on the purpose and design of the phantom; for a very small object, for instance, r.f. inhomogeneities are unlikely whereas for a large homogeneous phantom, susceptibility matching is of minor consequence.

It may also be beneficial if the structures of the phantom are discernable in computed tomography (P2) which means that the vessel and (all of) the MR signal source(s)

should be of different mass densities. Another, purely practical, addition to the solution is a preservative or disinfectant; as an example, NaN_3 is used in the Stanford Agar Phantom Recipe to "retard the growth of evil green things" (Friedman and Glover 2006).

The defining factor of an fMRI phantom is the *MRI signal modulator*. Different modulation techniques were already reviewed above; here I will concentrate on current-induced modulation of the magnetic field (for reasons to use such phantoms in the present study, see section P1: Feasibility of fMRI phantom with current-induced dephasing in Chapter 4). The pertinent issues can be divided into partially overlapping categories: MRI compatibility, signal modulation quality, MRI signal quality from the phantom, signal modulation geometry, and mechanical or assembly issues.

MRI compatibility (Schenck 1996) is of course the foremost consideration. To induce magnetic fields requires current conductors (for induction coils and potentially power cables), which—as unintended effects—can pick-up r.f. energy from the excitation pulse and thereby heat the conductor, or focus the r.f. excitation. The primary safety concern of fMRI phantoms occurs when the conductor resonates with the r.f. field. As a general rule, a resonance occurs if the length of the conductor is approximately equal to an integer multiple of half-wavelength of the r.f. field (Vernickel *et al.* 2005), but the geometry, connected components, position in the r.f. coil, *etc.* modify the resonance frequencies. In addition, the electrical permittivity of the signal medium affects the wavelength of the r.f. field, which concerns especially wires submerged in the medium. Therefore, experimental verification of safety is always required.

A related issue concerns the quality of signal modulation. As rapidly changing magnetic fields induce currents into nearby conductors, the coils of the signal modulator are also at risk of generating unknown currents, and consequently uncontrolled magnetic field modulation at the signal medium. Further, when current is applied to the induction coils of the signal modulator, the coil and the lead-wires are subject to Lorentz forces and torque that can move them if they are not attached firmly or wound appropriately (*e.g.* coaxial and twisted arrangements can be used). Moving current-carrying conductors obviously cause variable extraneous magnetic fields that degrade the image quality, affecting also the signal intensity measured from the fMRI phantom.

MRI signal quality from the phantom is mostly defined by the vessel and the signal medium. However, improper wiring geometry may disturb images. If the induction

coil of the signal modulator is submerged in the MR signal source, quite severe partial volume effects may take place. It follows that the phantom-induced field modulations influencing the spatial encoding of signal can effectively "move" signal to the volume occupied by the conductor, thus creating a large contrast to that volume; the signal would now seem to emanate from a location, which gave no signal prior to the modulation. Moreover, if the material of the coil is not susceptibility-matched with the signal medium, the coil will naturally deteriorate the image. If partial volume effects cannot be avoided, they can be minimised by using thin conductors, or even electrolytic conductors that are MRI signal sources themselves, as has been done in demonstrating magnetic resonance current density imaging (Joy *et al.* 1989). It is to be noted that if the conductor is placed beside the vessel in the transverse direction, the r.f. field cannot penetrate it, and the image suffers from intensity variations.

The signal modulation geometry defines the usability of an fMRI phantom. The alignment in which the phantom will reside in the scanner must be decided early on, because only the z-component of the induced $\mathbf{B}$ matters. The Biot–Savart law can be used to calculate the magnetic field distributions arising from various winding geometries. Whether the coil has to be "shielded", meaning that compensatory windings are included to reduce the signal modulation outside the fMRI phantom, depends on the intended applications. Eq. 7 provides the basis for MRI signal estimation based on the field pattern, *i.e.* how much dephasing will occur at each voxel. The Bloch equation (Eq. 5) provides for a more complete simulation framework.

And finally, the phantom needs to be assembled; it really can be the ship in the bottle if the eventual put-together is not borne in mind when designing the construct.

3 Objectives

The objectives of this thesis were to develop new experimental means to study fMRI signals without resorting to human (or animal) subjects, to illustrate application areas where such means would be useful, and to apply such means to demonstrate, verify, and discover information on some outstanding problem of importance. Specific aims were:

- to devise and test the feasibility of using electric current to induce magnetic field modulation in introducing fMRI activations *in vitro*, in an fMRI phantom (P1 & P3)

- to develop means to study localisation distortion of the fMRI imaging technique (P2)

- to use an fMRI phantom to simulate and study temporal signal properties at transitions between active and rest conditions, as in the brain (P4)

4   Summaries of studies

This chapter summarises the findings of the publications constituting the material of this dissertation after a concise account on employed methodology.

Materials and methods

All the experiments were carried out at the Advanced Magnetic Imaging Centre of Aalto University School of Science and Technology, and a 3-T General Electric Signa-series scanner was used in all MRI (the exact model, peripherals *etc.* varied, as indicated in the respective studies P1–P4, as a result of system upgrades).

The principal imaging method was manufacturer-provided GRE EPI-based fMRI although other MRI modalities were applied at times.

All studies involved construction of phantoms (Fig. 5), which were also the imaging targets in the respective works. Additionally, brain images were acquired in P2.
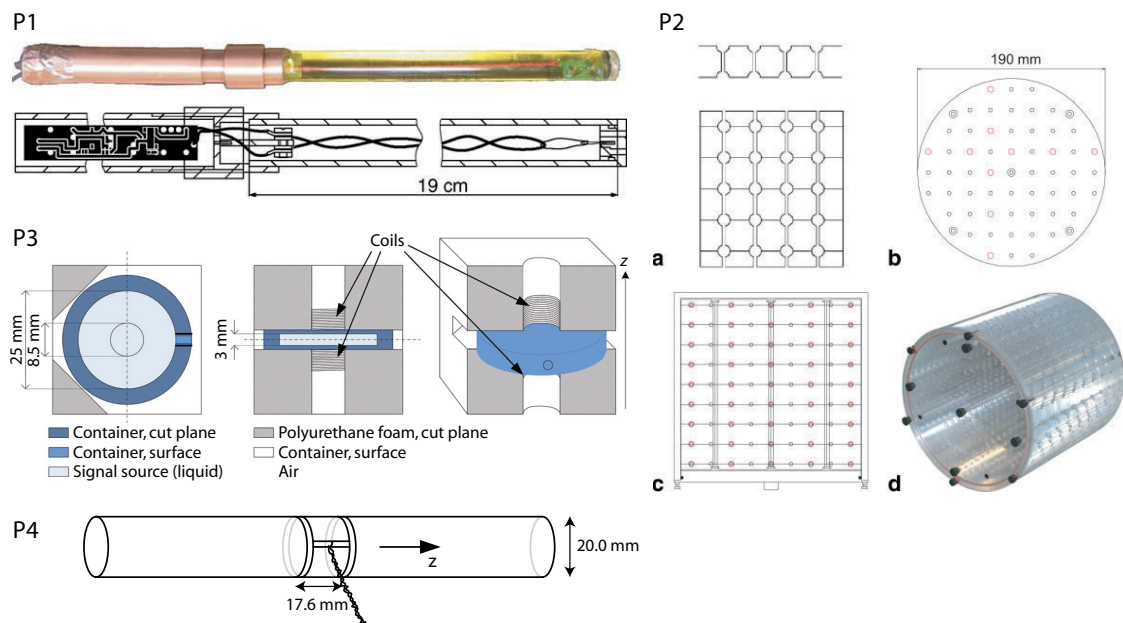
Figure 5: Pictures of the phantoms developed and used in the studies as indicated by the publication identifiers. The publications include detailed descriptions of each.

The work was carried out over an extended period of time and published in several papers; still the parts form a continuum. The investigation started out (P1) with testing the feasibility of an electrically operated fMRI phantom. Then it went on (P2) to a study of features of fMRI imaging, involving also determination of desired qualities in a phantom for EPI-based fMRI studies, which helped when (P3) the structure of the fMRI phantom was improved (and the modified phantom used to test some temporal characteristics of activation signal). Finally (P4), yet other modifications to the fMRI phantom, based on previous experience, were used to extract information on fMRI signal that could have implications on the analysis of certain types of human fMRI studies. Mostly, thus, the work comprised equipment and methods development.

I will now describe the individual studies and, finally, summarise and discuss the main results. The publications, included as appendices, contain the details of each study.

P1: Feasibility of fMRI phantom with current-induced dephasing

The fMRI signal relates with the transverse magnetisation of the sample and is, thus, a function of T_1, T_2, ρ, and especially magnetic field homogeneity. Notably, the signal does not "care" about the origins of these variables; if they occur similarly via two different mechanisms they are the same for the scanner.

In the brain, the fMRI signal changes because of modulations of oxygenation. The main component of the BOLD response is due to changes of local field homogeneity, such that spins in or near deoxygenated blood precess at a slightly higher frequency than those in oxygenated blood. These signal changes occur at a microscopic scale, but eventually they result from locally varying magnetic field homogeneity. These differences are addressed in more detail in the Discussion.

In the phantom used in the study, a local magnetic field was introduced in the sample by means of electromagnetic induction. A twisted carbon fibre was submerged in vegetable oil inside an elongated tubular vessel (Fig. 5, P1). Applying current to the fibre introduced some B_z in its vicinity; the field was inhomogeneous both axially, due to the twisting, and radially, decreasing in the second power of distance from the fibre, both with respect to the axis of the helices of the twist (and the vessel).
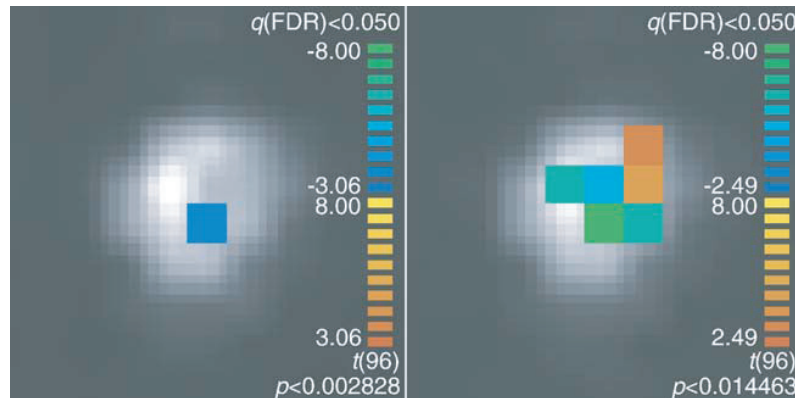
Figure 6: Statistically significant changes produced by applying a current of 0.3 mA (left panel) and 1.3 mA (right panel) in the conducting wire immersed in the centre of the vessel filled with the signal medium in 30-s ON/OFF-blocks. The in-plane size of the voxels shown as the coloured squares was 3.125×3.125 mm^2. The grey underlays illustrate the cross-section of the phantom. Fig. 2 of P1 shows the magnetic fields induced by the levels of inducing current. (Fig. 3 in P1)

It was shown that the fMRI signal decreased locally as the absolute value of intra-voxel B_z homogeneity decreased, as was deemed analogous with fMRI signal changes *in vivo*. When using a low current to induce activations, the phantom produced similar responses than are measured in human fMRI. Consequently, the feasibility test was successful, demonstrating that current-induced responses are relevant for physically simulating fMRI.

However, as the induction wire passed through the MR signal source, and because accurate positioning of the image stack was difficult, the functional point-spread function could not be evaluated using the phantom, as was originally thought. In particular, it would have been necessary to be able to align the image stack so that the wire would have passed only centres of voxels. The localiser image did not, however, provide a reliable reference for prescribing the EPI images due to geometric distortion, and different spatial encodings. Further, with the higher current level, the activation map shows both positive and negative voxels, as illustrated in Fig. 6. The reason is most likely a partial volume effect influencing both, the vicinity of the wire, and the edges of the phantom, where potentially large signal differences occur as a result of even a minute spatial encoding modulation. Similar effect has been noticed in another fMRI phantom experiment (Koopmans *et al.* 2004), with no explanation, but the reason could be the same as here. Another explanation is accidental local *correction* for susceptibility gradients at the vessel–signal-medium boundary. By the use of

spatial smoothing, all the activated voxels turned negatively correlated with the stimulus, which can be taken as a warning against excessive signal pre-processing.

The temporal and low-current measurements, however, provided results allowing us to consider that simulating activations with a current-based phantom is feasible.

P2: Quantification of geometric distortions

As an application of the EPI imaging method, fMRI is prone to severe geometrical distortions. To be able to account for the appearance, and to justify post-acquisition image deformations of fMRI component images, one needs to know how an accurately characterised object appears in the images. Ordinary structural and unstructured phantoms are of limited usability because they either do not show regular structure, contain too detailed structure, or possibly do not appear in the images at all (structured), or provide ambiguously interpretable information (unstructured).

Existing and available phantoms were deemed suboptimal for characterisation of EPI distortions, and thus a new phantom was designed and implemented. The phantom was crafted in phases. First the general properties of the vessel were determined by a series of trials. Then the vessel structure was designed and machined, and an appropriate filling was chosen.

As the nominal resolution of fMRI is often rather low (typically about 3 mm in x', y', and z'), the structures in an appropriate structural phantom must be large and separated by considerable distances. The size requirement follows from the need to be able to approximate the locations of the structures accurately, which requires a sufficient number of voxels, so that a reliable "centre of mass", representing the location of the structure, can be evaluated. Large distance between the structures was necessary for reliable discrimination of the signal from distinct compartments, because the EPI images tend to be blurred and distorted (see the leftmost panel in Fig. 7 for such an example). Also, geometric distortion of a few mm, and moderate susceptibility artefacts should be tolerated, so that the structures remain unambiguously discernable from each other, especially in the problematic phase encoding direction.

Plastic plates with several cylindrical holes served in figuring out appropriate compartment sizes and separations for the phantom structures. The actual phantom was designed and crafted accordingly: equidistant spheres, connected by thin capillaries, in the three rectangular directions filled with MR signal source (Fig. 5). The surface tension of the signal source was lowered by washing powder, so that after initial
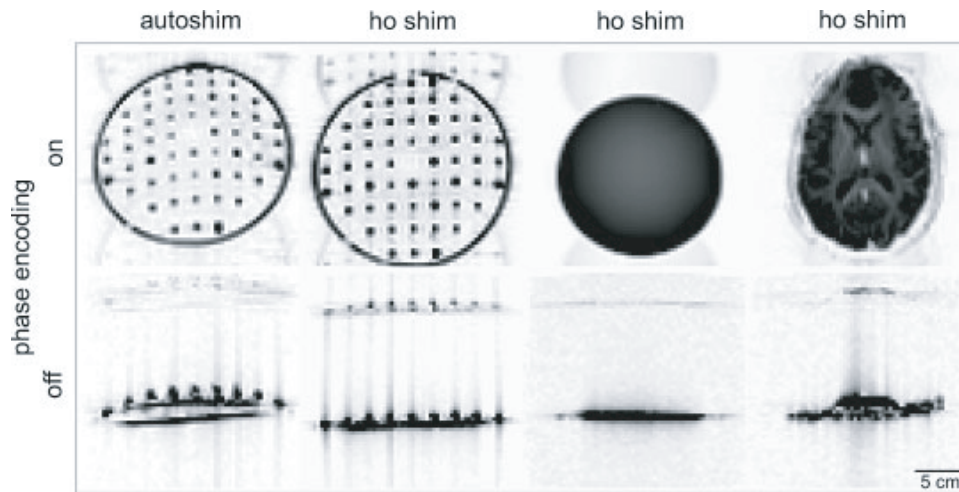
Figure 7: Zeroing the phase-encoding gradient gives a visual and quantitative window to inhomogeneities. The vertical direction in the lower row is encoded only by deviations from homogeneous B_0. Application of autoshim and high-order shim (ho) in the images is indicated. (Fig. 7 in P2)

bubble formation within the medium, the phantom's filling remained stable for several months. The stability of the filling was improved by initially lowering the pressure of the air remaining in the phantom. Thus, air bound to the signal medium and surfaces bubbled away and the filling could be completed by adding some more liquid before securing the cap.

In MRI, the user can combat image distortions by meticulous shimming. The use of mere "autoshimming" may be justified in clinical imaging in high-throughput settings, but given the distortion-vulnerability of EPI, fMRI should always be accompanied by more careful B_0 homogenisation; in MRI, shimming corresponds to calibrating the instrument to accommodate the measurement at hand. However, high-order shimming is not always feasible due to the limitations of the user interface of the magnet console.

Autoshimming, as compared with shimming the image volume by so-called high-order shim coils, resulted in seriously increased distortion (Fig. 7, two panels on the left). High-order shimming reduced distortion so that the shimmed phantom appeared very similar to an image acquired with autoshimming, after it had been transformed to correspond an anatomical image. If the image is devoid of distortions to begin with, a true one-to-one correspondence can be achieved between the source images and the image registration coordinates, for instance. If the signal in image locations is
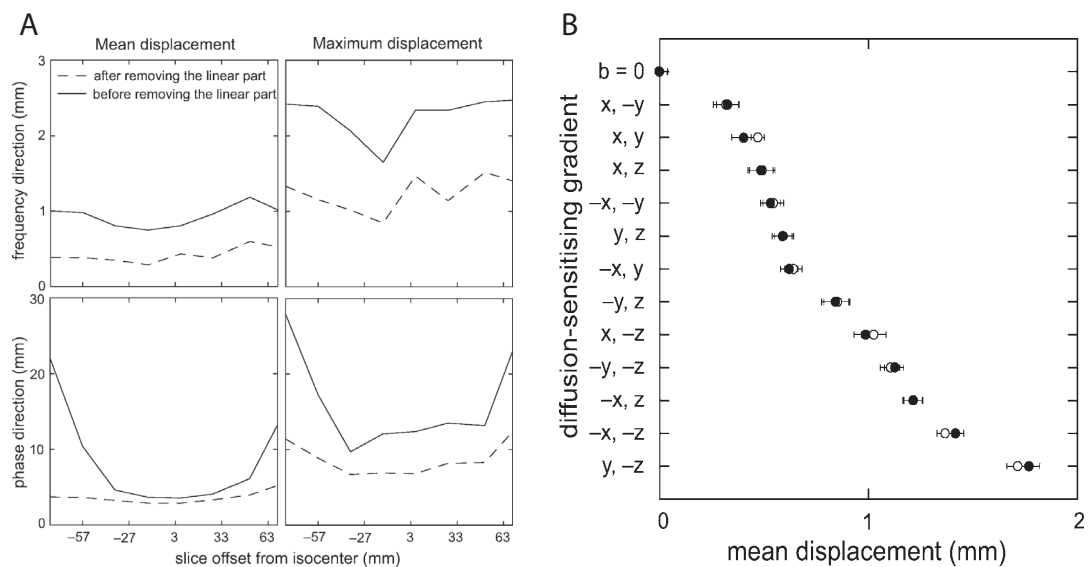
Figure 8: Geometric distortion in EPI. (A) Geometric distortion as a function of encoding direction and slice position in a fMRI pulse sequence. (Fig. 4 in P2) (B) Geometric distortion in diffusion tensor imaging was dependent on the direction of the diffusion-sensitising gradient. (Fig. 5 in P2)

"folded", *i.e.* originates from an anatomically different area than where it is encoded, such registration may lead to severe localisation errors.

A method employing the standard EPI sequence, but with manually zeroed phase-encoding gradient amplitudes, turned out to be a practical means to study and visualise the impact of poor field homogeneity. When the phase-encoding gradients are off, only the inhomogeneity gradients encode the phase direction. Thus, by observing the resultant images, the spread along the phase-encoded direction informs about the absolute field inhomogeneity, because in perfectly homogeneous field, a sample of a single spectral species (*e.g.* water) would yield a straight line in the frequency-encoded direction, where all signal would be aggregated (Fig. 7).

Without meticulous shimming, geometric distortions in EPI can be severe, as could be measured by the phantom. In the phase-encoding direction, the distortion depended on the slice, and differences exceeding 20 mm were found between the least distorted and maximally distorted structures. The structures within slices at the isocentre of the magnet were on average 15 mm less distorted in the phase-direction than structures residing on slices on the edges of the image stack. More surprisingly, the frequency-encoded direction was distorted as well by as much as 0.5–2 mm, with distortion depending on slice (Fig. 8A). In diffusion tensor imaging, the distortion depended on the direction of diffusion sensitising gradient, which may be detrimental for the proper

determination of the diffusion tensors (Fig. 8B). All of these exemplaries prompt for testing imaging methods to be used in fMRI by a phantom. The distortion may not be as easy to detect and characterise from the brain images, but is quite effortlessly obtainable using this phantom optimized for fMRI imaging sequences.

P3: Activation amplitudes in a compact fMRI reference phantom

In P3, another fMRI phantom, featuring a very compact signal medium compartment was built. The vessel held a 3-mm thick (z-direction) cylindrical liquid compartment of 25-mm diameter (Fig. 5). The thickness of the plastic enclosure was 1 mm in the z-direction, which implied that air surrounded the signal source at a very close distance, exposing the phantom to severe susceptibility gradients. However, as the MR signal modulator was brought outside the vessel, and installed on its z-surfaces, a thicker capsule would have degraded uniformity of the dephasing gradient field within the phantom. Therefore, the induction coil yielding the MR-signal modulation was mounted to a block of polyurethane foam (mostly air), because then the empty space left by the mould defining the geometry of the coil was surrounded by minimal amount of solid material. In practise, the foam was moulded onto the coil. This procedure resulted in the least complex susceptibility gradients that were attainable for the phantom.

These choices, however, left the MR-signal source in the close proximity of air. As the χ_m of water is lower than of air, the susceptibility gradients dephased the spins, and the signal measurable from the phantom was geometrically distorted.

Adding traces of Gd-based contrast agent to the water increased the susceptibility of the solution. Consequently, an optimal point for the χ_m was found where the signal from the phantom was close to maximum attainable, and the phantom was geometrically relatively undistorted. The χ_m of the resulting solution was approximated by the use of Wiedemann's law (Mulay 1963), and the applicability of the law was confirmed by observing the quantitatively correct shifts of the phantom's location in the phase-encoded direction as a function of concentrations of the solute.

In study P3, also a new transceiver was developed for signal delivery from the computer controlling the MR signal modulation to the phantom. The transceiver was tested and found to be MRI compliant in the 3-T environment. It was later reused to control the phantoms employed in P4.
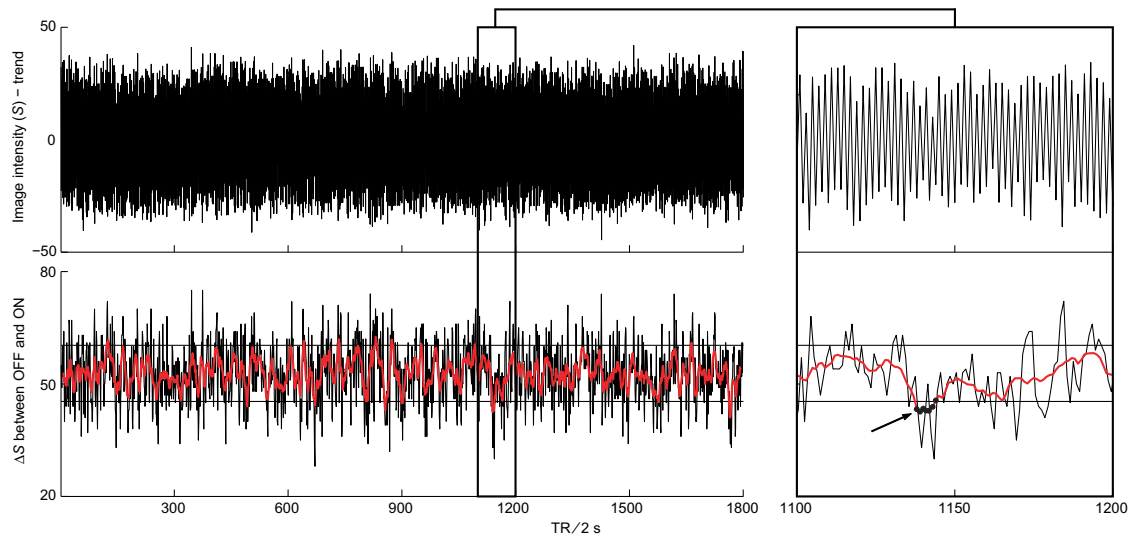
Figure 9: Measurement of activation stability. The top panel shows the image intensity from which a baseline has been subtracted during an experiment where B_z modulation (ΔB_z) was "OFF" and "ON" every other TR. The bottom panel shows a 10-point moving average of difference between the "OFF" and "ON" levels, horizontal lines indicate mean $\pm \sigma$ calculated over the whole measurement. Both the signal and the activation levels were very stable, with few crossings of the σ. (Fig. 6 in P3)

As an application of the phantom, the activation amplitude was traced during a long fMRI scanning. In the measurements, the scanner produced a stable signal, and no major discrepancies in activation amplitudes were detected (Fig. 9). However, as the phantom apparently produces stable activations, statistically significant deviations from constant activation amplitude would pinpoint periods when simultaneously measured brain fMRI data could be corrupted.

The design of the phantom described in P3 was preceded by several other attempts to use, *e.g.* rectangular and other more complex enclosures. All this preliminary work prompted the importance of χ_m at 3 T.

P4: Evidence of overshoot and undershoot transients at step transitions of fMRI activation

In P4, we studied a spin saturation effect (explained below) in the context of fMRI. In the real brain, the signal modulations are direct consequences of BOLD B_z changes. However, these changes are not considered as sources of actual artefacts but rather regarded as T_2^* modulators that additionally bring about some sharpening of signal localisation during positive BOLD responses.
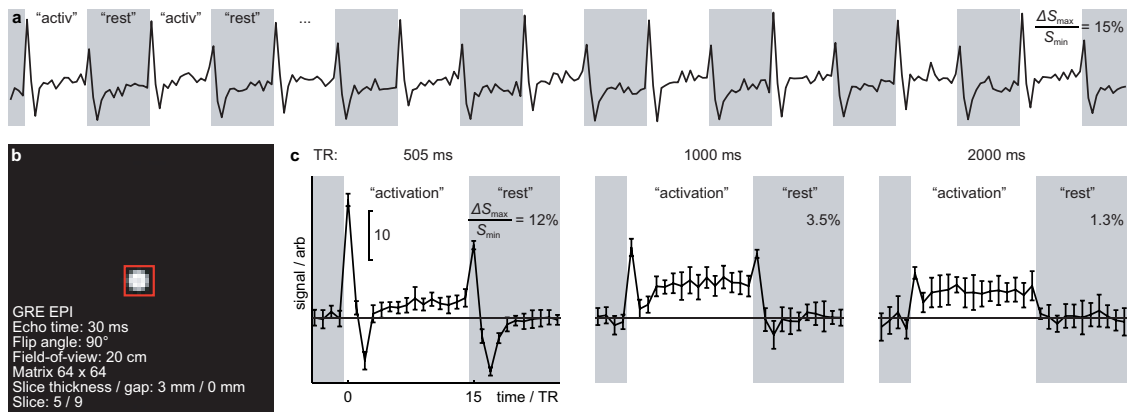
Figure 10: Transient over- and undershoots occurring in the fMRI signal whenever magnetic field changes. The field modulations in the experiment were step-transitions of B_z between "OFF" (activation) and "ON" (rest). The traces (c) show mean $\pm \sigma$ ($n = 9$) of the average signal from the ROI indicated by a red square in the transverse EPI slice of the phantom. Time scales for (c) are given in steps of three distinct TRs, as indicated. As an example, (a) expands the data collected in the leftmost panel of (c). (Fig. 2 in P4)

As the fMRI signal arises from oxygenation changes within a complex microstructure, it may go unnoticed that the field change during activation is, on average, always in the same direction, because the change of a linear χ_m scales $\mathbf{B}$. Therefore, the BOLD change of B_z not only randomly alters T_2^*, but also genuinely changes the field.

B_z changes between successive TRs distort the spatial encoding at the activated voxels because, due to superimposition of this bias on the slice selection gradient, slice selection targets different spins. Now, when the slice of spins affected by identical excitation pulses changes between two scans, longitudinal relaxation of the sample no longer commences from the same steady initial value than before, as has been noted and corrected for bulk motion (Friston *et al.* 1996; Muresan *et al.* 2002; Muresan *et al.* 2005; Kim *et al.* 2006; Bhagalia and Kim 2008; Kim *et al.* 2008), and in effect, the longitudinal magnetization starts to evolve toward a steady state after each change of B_z, similarly as in the beginning of an fMRI experiment. Therefore, depending on TR, it may take several scan repeats before the signal stabilizes again.

The change of B_z was physically modelled on two fMRI phantoms; Fig. 5 shows the general design, the difference between the two was the winding direction of one of the coils. One phantom induced a gradient field to cause dephasing, and the other induced a constant additional magnetic field (no dephasing, Fig. 10). The constant field alterations were simulated computationally as well.

The experiments and the computational simulations demonstrated that following a step-modulation of magnetic field between two successive scans of an image plane, transient over- and undershoots can occur in the fMRI signal time-course. The transient deflections were shown to arise from the finitely steep excitation slice profile.

The finding has potential implications on the interpretation of fMRI signal transients. If the fMRI signal can over- or undershoot in the absence of a corresponding physiological response, physiological modelling of haemodynamic response on the basis of fMRI signal can go awry.

5   Discussion

In this dissertation, I have presented four studies employing artificial imaging objects, *phantoms*. Because phantoms and humans are alike from the "scanner's point of view", both receiving and emitting MRI signal, phantoms provide intimate counterparts to *in vivo* measurements, more so than, *e.g.* computational simulations. While computer simulations are helpful, a physical model cannot overlook any hidden properties of the imaging process.

The role of phantoms for functional MRI

Three of the studies involved *fMRI phantoms*. The correspondence between these and human subjects, now as activations are considered, is less clear. Several differences are immediately recognised, starting with the functional signal generation mechanism, but similarities exist as well. Human BOLD responses occur through a haemodynamic response, and eventually the changes of blood oxygenation pertain to the signal changes. Also, no MRI-detectable BOLD signal could arise if B_z did not vary and further, the levels of the oxygenation, signal, and B_z all shift consistently either up or down during activations. These observations provide a level of justification for physically simulating fMRI by B_z adjustments of macroscopic range. Of course, the effect of interest determines whether an fMRI phantom provides a valid surrogate, and the extent of applicability of the physical simulation.

Our structural phantom to quantify geometric distortion in EPI (P2) is an example of an application-specific phantom. While many properties of MRI can be adequately confirmed by general-purpose phantoms, specific need is best served with specialised equipment. With the EPI-optimised structural phantom, we characterised distortions accurately and quantitatively, as was demanded. The requirement of specificity even accentuates with fMRI phantoms. *E.g.*, a spatially focused simulation of activation limits the spatial averaging potential and may impede certain temporal analyses. Conversely, a wide activation with gently-sloping boundaries would be useless in characterising the spreading of focused activations. A dephasing phantom is

suboptimal for studies of field shifting *etc*. While phantoms can be operose to construct, an expedient phantom serves the purpose best.

Quality assurance

If head motion-dependent signal changes from the phantom were detrended, a phantom could possibly act as a useful reference during the acquisition of a single subject's within-session data. The rationale for using a phantom to control within-session variability is basically the same as for any quality assurance: While (technical) signal abnormalities are rare, when they occur and are detected, possibly even accurately characterised and compensated, the examinations are better off than without the detection. Furthermore, a within-session reference phantom provides consistent activations throughout the imaging, so that a data quality check can be obtained from a well-defined location instead of analysing a larger ROI. Moreover, for instance in a hypothetical clinical condition in which the patient's activations are abnormal, or when rescanning at some later date is not possible (say, because a surgical operation based on the data had already been carried out), an activation reference would be valuable. A reference comes, however, at the expense of increased field of view, number of slices, or coil dimensions.

Reproducibility of fMRI activations still needs close attention, and individual subject variation, between-site variation, and between-subjects variation are regularly questioned. For instance, Zandbelt *et al.* (2008) report that individual fluctuations of activations are substantial, but group-level BOLD signal changes are stable over sessions. As another example, Gountouna *et al.* (2010) report that activations between different MRI scanners and sessions are well reproducible, while inter-subject variation is large. So perhaps equipments are improving and multi-centre studies have become feasible and reliable. Still, Friedman *et al.* (2008) are quite critical in evaluating multi-centre collaborative studies, reporting of multiple adjustments needed for experiments to produce repeatedly similar data, even with a simple and robust sensory-motor paradigm. An fMRI phantom could conceivably provide for objective control of *instrumental* variation by providing a much more stable yardstick than repeatedly scanning the same human subjects, enabling better focused psycho-physiological investigations on variability. The real utility of fMRI phantoms in quality assurance remains to be validated in practise.

Susceptibility issues

All fMRI phantoms constructed for this thesis work were rather compact. Controlling the EPI-related distortion in so small objects was challenging and in many instances material choices had but one parameter of relevance, susceptibility. A larger phantom would enable easier detection of current-induced signal changes (Bodurka *et al.* 1999). Nevertheless, in all fMRI works (P1, P3, P4) more reasons existed for keeping the vessels small than to make the construction easy. In studies P1 and P3, the phantoms were small enough for their eventual placing beside a human subject. In P4, the geometry of the induction coil necessitated a rather small diameter for the phantom because else a strong current (and unsafely long wires) would have been required to implement the physical simulation.

Although other means to accomplish the same exist, an inverse procedure of the susceptibility matching scheme outlined in Summaries of studies (P2) could have been useful for material selection, simultaneously quantifying often hard-to-find magnetic susceptibilities of prospective phantom materials. Immersing a piece of the material in water and subsequently gradually adding a solute of known χ_m while observing distortion-sensitive MR-images, *e.g.* obtainable by GRE EPI, would have come to a point where the object appears undistorted. The χ_m of the solution at that point would equal that of the material and the material's usability could have been easily resolved.

Absence of transients in unnatural physical situations

In study P4, the transients in the phantom were shown to arise from B_z shifts, with amplitudes depending on the rate of change. But why did measurements on phantom constructions of studies P1 and P3 not reveal such transients? In P1, the induction coil was a twisted electrical wire immersed within the signal medium, thus both partial volume effects and irregular field distribution undermined the shifts, because partly self-compensating as B that varied in both $-z$- and z-directions. In P3, as a result of susceptibility matching using Gd, the T_1, of the signal medium was very short, and hence spin saturation effect did not occur with the TRs used. In contrast, the signal medium in P4 had a long T_1 of ~2600 ms, which facilitated the generation of the transients. However, additional measurements (unpublished) on a signal medium with $T_1 \approx 1150$ ms yielded strong transients as well, yet the percent signal changes of the transients were weaker for TR = 1000 and TR = 2000. In the works of others, the r.f.-focussing phantom of Zhao *et al.* (2003) is not sensitive to the slice selection artefact, because it does not modulate the B_0-field. The transients are not relevant in the gel-

swapping phantom of Olsrud *et al.* (2008) either, although a somewhat similar bulk-motion effect occurs – they correct for it.

Furthermore, while the studies P1 and P3 concentrated on producing fMRI activations, the setup of the homogeneous phantom in P4 did not induce (much) dephasing. Possibly, however, some of the earlier data have contained these transients but have not caught the eye for any of the several possible reasons, foremost being that with step responses and longer TRs the effect is not so prominent. Another reason could be that transients in the signal are usually not welcomed, when encountered a possible step is to filter the input signal, which here would reduce the rate of change of B_z and consequently to eradicate the visible transients. While the transients were evident with both gradient and uniform B_z-modulations, in the uniform case the effect was quite conspicuous. Notwithstanding, study P4 showed that unaccounted HRF-type signal components can exist and that they can be retrieved by physical simulation.

Methodological contemplations

In addition to what has already been discussed about P1, the signal medium was rather randomly chosen. While it did not affect the reported measurements completed soon after its assembly, in time it would have become rancid and thus not remain stable. Also, the carbon lead wire immersed in the signal medium was not optimal. Because of extreme difficulties in acquiring proper yarn, the lead wire had to be separated from a fabric and insulated by hand, whereby the wire took up more space than would have been desired, and its structure was somewhat irregular. The foremost issue in P1 was, however, the inhomogenising magnetic field being created by an immersed wire, because thereby dissecting useful (uncontaminated by partial volume effect) voxels from the phantom became problematical.

The biggest issue of the fMRI phantom in P3 was the chosen geometry. Whereas the phantom itself gave relatively (EPI perspective) undistorted signal of sufficient amplitude, it failed to reflect some aspects of physiologically valid physics, because the signal medium was squeezed into a 3-mm thick compartment. The contribution of the adjacent space, as was shown later, can be rather consequential for natural signal formation. Additionally, as with any compact phantom, local shimming effects can happen at the vessel–signal-medium boundary with modulated B_z, which would cancel some of the intended inhomogeneity effect. However, it was not the purpose of the phantom to be a physiology simulator but rather offer a reference for potential dephasing amplitude alteration.

It seems remote to attempt to calibrate between brain activation measurements using an fMRI phantom measured *simultaneously* with a subject. To obtain comparable signals from a phantom in different imaging sessions, while simultaneously acquiring signal from the brain appears even harder than to obtain commensurate signal(s) from the brain(s) alone. The phantom will necessarily reside in the less homogeneous regions of the B_1-field, the B_0-field is shimmed according to the brain to acquire the best possible brain data. Moreover, different subjects' heads (or the same subject's head on different days) will load the coil and inhomogenise the field differently, all of which will effectively render the fMRI signal from the phantom much harder to equalise than the brain data ever.

The spin-saturation model quite successfully predicted the shapes of the transient responses. Including more parameters could, however, improve the accuracy of the simulation, which will be considered in future work. To improve the experimentally testable repertoire of hypotheses, a more versatile transceiver would be needed to feed the phantom. The current transceiver has only two modes, on and off, which clearly does not allow many additional experiments. Furthermore, knowing the true excitation profile throughout the phantom would enable more accurate simulations.

Future topics

Printed circuit board phantoms

To minimise the interference of support structures, and to improve durability and accuracy, phantoms made of printed circuit board would be useful. As also flexible circuit boards allowing non-planar geometries are available, the compromises due to this material choice would be limited.

Investigation on the significance of the "unphysiological" transients in humans

The implications of the slice artefact transients on human fMRI remain to be seen and tested. How strong this effect ultimately is in humans and whether it relates to the observed human fMRI over- and undershoots and the initial dip still remains to be studied. In the phantom measurements and computer simulations of P4, the slice selection error due to B_z modulation was, even though of physiologically rooted magnitude, wide and smooth. At least the spatial pattern of activations within a voxel is unlikely symmetric on the z-borders of a slice, nor distributed over the whole voxel. The transient increase of signal in the phantom does not necessarily translate directly to the brain data of humans.

50

Enhancement and suppression of transients

As discussed in P4, ways exist to enhance or suppress the transients, and to test whether or not these spin saturation transients pertain to human BOLD signal transients. An easily conceivable procedure (discussed to some extent in P4) is to reduce the amplitude of the slice selection gradient, while keeping other things equal because that way the B_z modulation becomes relatively stronger. Reducing the gradient and adjusting the r.f. pulse correspondingly is one possibility. However, an immediately available method, of which initial steps have already been taken, is to tilt the slice planes from axial toward coronal or sagittal through an angle θ. Thus G_z reduces by a factor of $(1 - \cos\theta)$. However, with $\theta \approx \pi/2$ could imply signal shifts over several planes on slice borders, or signal translation within slices. Additionally, very small χ_m variation can then inflict signal mislocation between or within slices. Finally, although the importance of short TR in transient generation diminishes as the transition time of B_z rises, because the strongest phantom-produced transients and the initial dip both coincide with short TRs, experiments with TR as a variable cannot be neglected.

Looking for the initial dip

As reducing G_z can be envisioned a feasible way to increase the transients, the notion that the biggest initial dips have been observed with non-axial slices becomes interesting (Refs. in Table 1). We do not yet know how large an impact the effect has on human fMRI data, but simulations on physiologically valid parameter choices indicate that these unphysiological transients may require attention.

$\star$ $\quad$ $\star$ $\quad$ $\star$

Functional magnetic resonance imaging provides means to look at brain function through a signal informed of blood oxygenation. The signal, thus, only indirectly reflects neuronal activity, and it is not earmarked to bear information only of brain activations. Phantoms, designed, constructed, and tested in this dissertation, provide an attractive means for peeking at the signal. The principle of using phantoms to imitate the brain, including activations, was demonstrated viable, although the existing concepts can be refined and new application-specific instruments developed. The true relevance of the phantom findings for physiological interpretations remains to be validated. Still, these first steps carry a promise that phantom experiments, and phantom experiment-inspired fMRI studies on human subjects, will improve our understanding of human brain function.

Acknowledgements

I would also like to express my gratitude to the excellent administrative talents of Low Temperature Laboratory, Prof. Mikko Paalanen as the director of the Lab, Teija Halme, Tuire Koivisto, Leena Meilahti, Pirjo Muukkonen, and Liisi Pasanen. For technical support I would like to thank Doc. Veikko Jousmäki, Helge Kainulainen, Petteri Räisänen, Ronny Schreiber, and collectively the helpful gentlemen of the workshop.

I was fortunate to get to spend some two months with Prof. Gareth Barker of the Institute of Psychiatry, King's College London, to learn tricks of the trade of MRI. I am thankful to him as a friendly host and extraordinary tutor. There is, in my opinion, no better way to learn MRI than pulse sequence programming.

I would also like to thank Kikka Lilius, Jorma Linnanmäki, Eero Mykrä, Harri Pättikangas, and Markus Salonen from GE Healthcare for support.

Having spent many years in AMI Centre, it has been a genuine pleasure to share the time (and, for quite some time, office) with Marita Kattelus. Thanks Marita for your extraordinary company as well as all the assistance with measurements.

Fellow inmates, as you are quite a few, and as I cannot confidently guarantee 0% omissions, much less tolerate the shame for forgetting someone specifically, I would like to collectively cheer you all and thank for the good company.

In this penultimate paragraph, I would like to express my warmest thanks to all my family. My parents Pirkko and Seppo have always been supportive, and blissfully, sufficiently unintrusive of my work. I also take this chance to thank my mother-in-law Sisko for all the help in facilitating our day-to-day life whenever necessary. Most preciously, I thank Mirja for her encouragement and understanding. It is heart-rending to be aware of how distant and, frankly, not nice I have been to you and our kids Ukko and Ingrid as well, especially during the past few months. Sorry guys; and thanks!

Espoo, March 2010

Ville Renvall

Bibliography

Adam G, Glowinski A, Neuerburg J, Bücker A, van Vaals JJ, Günther RW (1998): Visualization of MR-compatible catheters by electrically induced local field inhomogeneities: evaluation in vivo. *Journal of Magnetic Resonance Imaging* 8(1): 209–213.

Ashburner J, Friston KJ (2000): Voxel-based morphometry—the methods. *NeuroImage* 11(6): 805–821.

Aso T, Urayama S-i, Poupon C, Sawamoto N, Fukuyama H, Le Bihan D (2009): An intrinsic diffusion response function for analyzing diffusion functional MRI time series. *NeuroImage* 47(4): 1487–1495.

Bakker CJG, de Roos R (2006): Concerning the preparation and use of substances with a magnetic susceptibility equal to the magnetic susceptibility of air. *Magnetic Resonance in Medicine* 56(5): 1107–1113.

Bandettini PA, Wong EC, Hinks RS, Tikofsky RS, Hyde JS (1992): Time course EPI of human brain function during task activation. *Magnetic Resonance in Medicine* 25(2): 390–397.

Bandettini PA, Wong EC, Jesmanowicz A, Hinks RS, Hyde JS (1994): Spin-echo and gradient-echo epi of human brain activation using bold contrast: a comparative study at 1.5 T. *NMR in Biomedicine* 7(1–2): 12–20.

Behzadi Y, Liu TT (2006): Caffeine reduces the initial dip in the visual BOLD response at 3 T. *NeuroImage* 32(1): 9–15.

Belliveau JW, Kennedy DN, Jr., McKinstry RC, Buchbinder BR, Weisskoff RM, Cohen MS, Vevea JM, Brady TJ, Rosen BR (1991): Functional mapping of the human visual cortex by magnetic resonance imaging. *Science* 254(5032): 716–719.

Belliveau JW, Rosen BR, Kantor HL, Rzedzian RR, Kennedy DN, McKinstry RC, Vevea JM, Cohen MS, Pykett IL, Brady TJ (1990): Functional cerebral imaging by susceptibility-contrast NMR. *Magnetic Resonance in Medicine* 14(3): 538–546.

Bernstein MA, King KF, Zhou XJ (2004): *Handbook of MRI Pulse Sequences*. Burlington: Elsevier Academic Press.

Bhagalia R, Kim B (2008): Spin saturation artifact correction using slice-to-volume registration motion estimates for fMRI time series. *Medical Physics* 35(2): 424–434.

Bloch F (1946): Nuclear induction. *Physical Review* 70(7–8): 460–474.

Bloch F, Hansen WW, Packard M (1946a): Nuclear induction. *Physical Review* 69(3–4): 127.

Bloch F, Hansen WW, Packard M (1946b): The nuclear induction experiment. *Physical Review* 70(7–8): 474–485.

Block KT, Frahm J (2005): Spiral imaging: a critical appraisal. *Journal of Magnetic Resonance Imaging* 21(6): 657–668.

Block W, Pauly J, Kerr A, Nishimura D (1997): Consistent fat suppression with compensated spectral-spatial pulses. *Magnetic Resonance in Medicine* 38(2): 198–206.

Bloembergen N, Purcell EM, Pound RV (1947): Nuclear magnetic relaxation. *Nature* 160(4066): 475–476.

Bodurka J, Bandettini PA (2002): Toward direct mapping of neuronal activity: MRI detection of ultraweak, transient magnetic field changes. *Magnetic Resonance in Medicine* 47(6): 1052–1058.

Bodurka J, Jesmanowicz A, Hyde JS, Xu H, Estkowski L, Li SJ (1999): Current-induced magnetic resonance phase imaging. *Journal of Magnetic Resonance* 137(1): 265–271.

Bottomley PA, Foster TH, Argersinger RE, Pfeifer LM (1984): A review of normal tissue hydrogen NMR relaxation times and relaxation mechanisms from 1–100

MHz: dependence on tissue type, NMR frequency, temperature, species, excision, and age. *Medical Physics* 11(4): 425–448.

Boynton GM, Engel SA, Glover GH, Heeger DJ (1996): Linear systems analysis of functional magnetic resonance imaging in human V1. *The Journal of Neuroscience* 16(13): 4207–4221.

Buxton RB (2001): The elusive initial dip. *NeuroImage* 13(6): 953–958.

Buxton RB, Uludağ K, Dubowitz DJ, Liu TT (2004): Modeling the hemodynamic response to brain activation. *NeuroImage* 23(Suppl 1): S220–S233.

Buxton RB, Wong EC, Frank LR (1998): Dynamics of blood flow and oxygenation changes during brain activation: the balloon model. *Magnetic Resonance in Medicine* 39(6): 855–864.

Cassará AM, Maraviglia B, Hartwig S, Trahms L, Burghoff M (2009): Neuronal current detection with low-field magnetic resonance: simulations and methods. *Magnetic Resonance Imaging* 27(8): 1131–1139.

Chen JJ, Pike GB (2009): Origins of the BOLD post-stimulus undershoot. *NeuroImage* 46(3): 559–568.

Chen W, Zhu X-H, Kato T, Andersen P, Uğurbil K (1998): Spatial and temporal differentiation of fMRI BOLD response in primary visual cortex of human brain during sustained visual simulation. *Magnetic Resonance in Medicine* 39(4): 520–527.

Cheng H, Zhao Q, Duensing GR, Edelstein WA, Spencer D, Browne N, Saylor C, Limkeman M (2006): SmartPhantom — an fMRI simulator. *Magnetic Resonance Imaging* 24(3): 301–313.

Cheng H, Zhao Q, Spencer D, Duensing GR, Edelstein WA (2004): A fMRI study of the smartphantom. *Proceedings of the International Society for Magnetic Resonance in Medicine* 11: p. 1041.

Damadian R (1971): Tumor detection by nuclear magnetic resonance. *Science* 171(3976):1151–1153.

Damadian R, Zaner K, Hor D, DiMaio T (1974): Human tumors detected by nuclear magnetic resonance. *Proceedings of the National Academy of Sciences of the United States of America* 71(4): 1471–1473.

Davis RS (1998): Equation for the volume magnetic susceptibility of moist air. *Metrologia* 35(1): 49–55.

Duong TQ, Kim D-S, Uğurbil K, Kim S-G (2000): Spatiotemporal dynamics of the BOLD fMRI signals: toward mapping submillimeter cortical columns using the early negative response. *Magnetic Resonance in Medicine* 44(2): 231–242.

Durand E, van de Moortele P-F, Pachot-Clouard M, Le Bihan D (2001): Artifact due to B_0 fluctuations in fMRI: correction using the *k*-space central line. *Magnetic Resonance in Medicine* 46(1): 198–201.

Edelstein WA, Hutchison JMS, Johnson G, Redpath T (1980): Spin warp NMR imaging and applications to human whole-body imaging. *Physics in Medicine and Biology* 25(4): 751–756.

Emir UE, Ozturk C, Akin A (2008): Multimodal investigation of fMRI and fNIRS derived breath hold BOLD signals with an expanded balloon model. *Physiological Measurement* 29(1): 49–63.

Fox MD, Snyder AZ, Barch DM, Gusnard DA, Raichle ME (2005a): Transient BOLD responses at block transitions. *NeuroImage* 28(4): 956–966.

Fox MD, Snyder AZ, McAvoy MP, Barch DM, Raichle ME (2005b): The BOLD onset transient: identification of novel functional differences in schizophrenia. *NeuroImage* 25(3): 771–782.

Frahm J, Baudewig J, Kallenberg K, Kastrup A, Merboldt KD, Dechent P (2008): The post-stimulation undershoot in BOLD fMRI of human brain is not caused by elevated cerebral blood volume. *NeuroImage* 40(2): 473–481.

Friedman L, Glover GH (2006): Report on a multicenter fMRI quality assurance protocol. *Journal of Magnetic Resonance Imaging* 23(6): 827–839.

Friedman L, Stern H, Brown GG, Mathalon DH, Turner J, Glover GH, Gollub RL, Lauriello J, Lim KO, Cannon T, Greve DN, Bockholt HJ and others (2008):

Test-retest and between-site reliability in a multicenter fMRI study. *Human Brain Mapping* 29(8): 958–972.

Friston KJ, Fletcher P, Josephs O, Holmes A, Rugg MD, Turner R (1998): Event-related fMRI: characterizing differential responses. *NeuroImage* 7(1): 30–40.

Friston KJ, Williams S, Howard R, Frackowiak RS, Turner R (1996): Movement-related effects in fMRI time-series. *Magnetic Resonance in Medicine* 35(3): 346–55.

Frostig RD, Lieke EE, Ts'o DY, Grinvald A (1990): Cortical functional architecture and local coupling between neuronal activity and the microcirculation revealed by in vivo high-resolution optical imaging of intrinsic signals. *Proceedings of the National Academy of Sciences of the United States of America* 87(16): 6082–6086.

Garroway AN, Grannell PK, Mansfield P (1974): Image formation in NMR by a selective irradiative process. *Journal of Physics C: Solid State Physics* 7(24): L457–L462.

Glover GH (1999a): 3D z-shim method for reduction of susceptibility effects in BOLD fMRI. *Magnetic Resonance in Medicine* 42(2): 290–299.

Glover GH (1999b): Deconvolution of impulse response in event-related BOLD fMRI. *NeuroImage* 9(4): 416–429.

Glover GH, Lee AT (1995): Motion artifacts in fMRI: comparison of 2DFT with PR and spiral scan methods. *Magnetic Resonance in Medicine* 33(5): 624–635.

Glover GH, Lemieux SK, Drangova M, Pauly JM (1996): Decomposition of inflow and blood oxygen level-dependent (BOLD) effects with dual-echo spiral gradient-recalled echo (GRE) fMRI. *Magnetic Resonance in Medicine* 35(3): 299–308.

Glowinski A, Adam G, Bücker A, Neuerburg J, van Vaals JJ, Günther RW (1997): Catheter visualization using locally induced, actively controlled field inhomogeneities. *Magnetic Resonance in Medicine* 38(2): 253–258.

Gountouna V-E, Job DE, McIntosh AM, Moorhead TWJ, Lymer GKL, Whalley HC, Hall J, Waiter GD, Brennan D, McGonigle DJ, Ahearn TS, Cavanagh J and

others (2010): Functional magnetic resonance imaging (fMRI) reproducibility and variance components across visits and scanning sites with a finger tapping task. *NeuroImage* 49(1): 552–560.

Guimares AR, Melcher JR, Talavage TM, Baker JR, Ledden P, Rosen BR, Kiang NYS, Fullerton BC, Weisskoff RM (1998): Imaging subcortical auditory activity in humans. *Human Brain Mapping* 6(1): 33–41.

Hahn EL (1950): Spin echoes. *Physical Review* 80(4): 580–594.

Harshbarger TB, Song AW (2008): Differentiating sensitivity of post-stimulus undershoot under diffusion weighting: implication of vascular and neuronal hierarchy. *PLoS ONE* 3(8): e2914.

Henriksen O, de Certaines JD, Spisni A, Cortsen M, Muller RN, Ring PB (1993): V. In vivo field dependence of proton relaxation times in human brain, liver and skeletal muscle: a multicenter study. *Magnetic Resonance Imaging* 11(6): 851–856.

Hiltunen J, Hari R, Jousmäki V, Müller K, Sepponen R, Joensuu R (2006): Quantification of mechanical vibration during diffusion tensor imaging at 3 T. *NeuroImage* 32(1): 93–103.

Hu X, Le TH, Uğurbil K (1997): Evaluation of the early response in fMRI in individual subjects using short stimulus duration. *Magnetic Resonance in Medicine* 37(6): 877–884.

Huettel SA, McCarthy G (2000): Evidence for a refractory period in the hemodynamic response to visual stimuli as measured by MRI. *NeuroImage* 11(5): 547–553.

Huettel SA, Song AW, McCarthy G (2004): *Functional Magnetic Resonance Imaging*. Sunderland: Sinauer Associates, Inc.

Hulvershorn J, Bloy L, Gualtieri EE, Leigh JS, Elliott MA (2005): Spatial sensitivity and temporal response of spin echo and gradient echo bold contrast at 3 T using peak hemodynamic activation time. *NeuroImage* 24(1): 216–223.

Janz C, Schmitt C, Speck O, Hennig J (2000): Comparison of the hemodynamic response to different visual stimuli in single-event and block stimulation fMRI experiments. *Journal of Magnetic Resonance Imaging* 12(5): 708–714.

Joensuu R, Renvall V, Hari R (2004): fMRI phantom for and MR imager [TH 296]. Budapest, Hungary. Organization for Human Brain Mapping. CD-ROM.

Jones RA (1999): Origin of the signal undershoot in BOLD studies of the visual cortex. *NMR in Biomedicine* 12(5): 299–308.

Jones RA, Schirmer T, Lipinski B, Elbel GK, Auer DP (1998): Signal undershoots following visual stimulation: A comparison of gradient and spin-echo BOLD sequences. *Magnetic Resonance in* Medicine 40(1): 112–118.

Joy M, Scott G, Henkelman M (1989): In vivo detection of applied electric currents by magnetic resonance imaging. *Magnetic Resonance Imaging* 7(1): 89–94.

Kato H, Kuroda M, Yoshimura K, Yoshida A, Hanamoto K, Kawasaki S, Shibuya K, Kanazawa S (2005): Composition of MRI phantom equivalent to human tissues. *Medical Physics* 32(10): 3199–3208.

Kim B, Bhagalia R, Yeo D (2006): A realistic fMRI time series simulation with individual slice motion, geometric distortion and spin saturation effect. *Proceedings of the International Society for Magnetic Resonance in Medicine* 14: p. 2391.

Kim B, Yeo DTB, Bhagalia R (2008): Comprehensive mathematical simulation of functional magnetic resonance imaging time series including motion-related image distortion and spin saturation effect. *Magnetic Resonance Imaging* 26(2): 147–159.

Kim D-S, Duong TQ, Kim S-G (2000): High-resolution mapping of iso-orientation columns by fMRI. *Nature Neuroscience* 3(2): 164–169.

Koopmans P, Lanting C, Versluis M, Hoogduin H (2004): Development of a reference phantom for fMRI studies. *Proceedings of the International Society for Magnetic Resonance in Medicine* 11: p. 1039.

Kumar A, Welti D, Ernst RR (1975): NMR Fourier zeugmatography. *Journal of Magnetic Resonance* 18(1): 69–83.

Kwong KK, Belliveau JW, Chesler DA, Goldberg IE, Weisskoff RM, Poncelet BP, Kennedy DN, Hoppel BE, Cohen MS, Turner R, Cheng H-M, Brady TJ and others (1992): Dynamic magnetic resonance imaging of human brain activity

during primary sensory stimulation. *Proceedings of the National Academy of Sciences of the United States of America* 89(12): 5675–5679.

Lange N, Zeger SL (1997): Non-linear fourier time series analysis for human brain mapping by functional magnetic resonance imaging. *Journal of the Royal Statistical Society Series C (Applied Statistics)* 46(1): 1–29.

Lauterbur PC (1973): Image formation by induced local interactions: examples employing nuclear magnetic resonance. *Nature* 242(5394): 190-191.

Lauterbur PC (1974): Magnetic resonance zeugmatography. *Pure and Applied Chemistry* 40(1-2): 149–157.

Le Bihan D, Urayama S-i, Aso T, Hanakawa T, Fukuyama H (2006): Direct and fast detection of neuronal activation in the human brain with diffusion MRI. *Proceedings of the National Academy of Sciences of the United States of America* 103(21): 8263–8268.

Levitt MH (2003): *Spin Dynamics: Basics of Nuclear Magnetic Resonance*. Wiltshire: John Wiley & Sons Ltd.

Li Y, Reza S, Limkeman MK (2007): Phantom calibration method for improved temporal characterization of hemodynamic response in event-related fMRI. *NeuroImage* 35(2): 566–576.

Liang Z-P, Lauterbur PC (2000): *Principles of Magnetic Resonance Imaging: A Signal Processing Perspective*. Akay M, editor. New York: IEEE Press.

Lindauer U, Royl G, Leithner C, Kühl M, Gethmann J, Kohl-Bareis M, Villringer A, Dirnagl U (2002): Neuronal activation induced changes in microcirculatory haemoglobin oxygenation: to dip or not to dip. *International Congress Series* 1235: 137–144.

Lindauer U, Royl G, Leithner C, Kühl M, Gold L, Gethmann J, Kohl-Bareis M, Villringer A, Dirnagl U (2001): No evidence for early decrease in blood oxygenation in rat whisker cortex in response to functional activation. *NeuroImage* 13(6): 988–1001.

Liu TT, Luh W-M, Wong EC, Frank LR, Buxton RB (2000): A method for dynamic measurement of blood volume with compensation for T2 changes. *Proceedings of the International Society for Magnetic Resonance in Medicine* 8: p. 53.

Ljunggren S (1983): A simple graphical representation of Fourier-based imaging methods. *Journal of Magnetic Resonance* 54(2): 338–343.

Logothetis NK, Guggenberger H, Peled S, Pauls J (1999): Functional imaging of the monkey brain. *Nature Neuroscience* 2(6): 555–562.

Lu H, Clingman C, Golay X, van Zijl PCM (2004): Determining the longitudinal relaxation time (T_1) of blood at 3.0 Tesla. *Magnetic Resonance in Medicine* 52(3): 679–682.

Lüdeke KM, Röschmann P, Tischler R (1985): Susceptibility artefacts in NMR imaging. *Magnetic Resonance Imaging* 3(4): 329–343.

Malinen S, Schürmann M, Hlushchuk Y, Forss N, Hari R (2006): Improved differentiation of tactile activations in human secondary somatosensory cortex and thalamus using cardiac-triggered fMRI. *Experimental Brain Research* 174(2): 297–303.

Malonek D, Grinvald A (1996): Interactions between electrical activity and cortical microcirculation revealed by imaging spectroscopy: implications for functional brain mapping. *Science* 272(5261): 551–554.

Mandeville JB, Marota JJA, Ayata C, Moskowitz MA, Weisskoff RM, Rosen BR (1999): MRI measurement of the temporal evolution of relative $CMRO_2$ during rat forepaw stimulation. *Magnetic Resonance in Medicine* 42(5): 944–951.

Mansfield P (1977): Multi-planar image formation using NMR spin echoes. *Journal of Physics C: Solid State Physics* 10: L55–L58.

Marota JJA, Ayata C, Moskowitz MA, Weisskoff RM, Rosen BR, Mandeville JB (1999): Investigation of the early response to rat forepaw stimulation. *Magnetic Resonance in Medicine* 41(2): 247–252.

McRobbie DW, Moore EA, Graves MJ, Prince MR (2005): *MRI from Picture to Proton*. Cambridge: Cambridge University Press.

Menon RS, Ogawa S, Hu X, Strupp JP, Anderson P, Uğurbil K (1995): BOLD based functional MRI at 4 tesla includes a capillary bed contribution: echo-planar imaging correlates with previous optical imaging using intrinsic signals. *Magnetic Resonance in Medicine* 33(3): 453–459.

Mildner T, Norris DG, Schwarzbauer C, Wiggins CJ (2001): A qualitative test of the balloon model for BOLD-based MR signal changes at 3T. *Magnetic Resonance in Medicine* 46(5): 891–899.

Miller KL, Bulte DP, Devlin H, Robson MD, Wise RG, Woolrich MW, Jezzard P, Behrens TEJ (2007): Evidence for a vascular contribution to diffusion FMRI at high *b* value. *Proceedings of the National Academy of Sciences of the United States of America* 104(52): 20967–20972.

Morrell G, Spielman D (1997): Dynamic shimming for multi-slice magnetic resonance imaging. *Magnetic Resonance in Medicine* 38(3): 477–483.

Mulay LN (1963): *Magnetic Susceptibility*. New York: Interscience Publishers.

Muresan L, Renken R, Roerdink JB, Duifhuis H (2002): Position-history and spin-history artifacts in fMRI time series. San Diego, CA, USA. SPIE. pp. 444–451.

Muresan L, Renken R, Roerdink JBTM, Duifhuis H (2005): Automated correction of spin-history related motion artefacts in fMRI: simulated and phantom data. *IEEE Transactions on Biomedical Engineering* 52(8): 1450–1460.

Ogawa S, Lee TM, Kay AR, Tank DW (1990): Brain magnetic resonance imaging with contrast dependent on blood oxygenation. *Proceedings of the National Academy of Sciences of the United States of America* 87(24): 9868–9872.

Ogawa S, Tank DW, Menon R, Ellermann JM, Kim SG, Merkle H, Ugurbil K (1992): Intrinsic signal changes accompanying sensory stimulation: functional brain mapping with magnetic resonance imaging. *Proceedings of the National Academy of Sciences of the United States of America* 89(13): 5951–5955.

Olsrud J, Nilsson A, Mannfolk P, Waites A, Ståhlberg F (2008): A two-compartment gel phantom for optimization and quality assurance in clinical BOLD fMRI. *Magnetic Resonance Imaging* 26(2): 279–286.

Park TS, Lee SY (2007): Effects of neuronal magnetic fields on MRI: Numerical analysis with axon and dendrite models. *NeuroImage* 35(2): 531–538.

Parkes LM, de Lange FP, Fries P, Toni I, Norris DG (2007): Inability to directly detect magnetic field changes associated with neuronal activity. *Magnetic Resonance in Medicine* 57(2): 411–416.

Petridou N, Plenz D, Silva AC, Loew M, Bodurka J, Bandettini PA (2006): Direct magnetic resonance detection of neuronal electrical activity. *Proceedings of the National Academy of Sciences of the United States of America* 103(43): 16015–16020.

Purcell EM, Torrey HC, Pound RV (1946): Resonance absorption by nuclear magnetic moments in a solid. *Physical Review* 69(1–2): 37–38.

Rice JR, Milbrandt RH, Madsen EL, Frank GR, Boote EJ, Blechinger JC (1998): Anthropomorphic ^{1}H MRS head phantom. *Medical Physics* 25(7): 1145–1156.

Roberts KC, Tran TT, Song AW, Woldorff MG (2007): Component structure of event-related fMRI responses in the different neurovascular compartments. *Magnetic Resonance Imaging* 25(3): 328–334.

Sadaghiani S, Uğurbil K, Uludağ K (2009): Neural activity-induced modulation of BOLD poststimulus undershoot independent of the positive signal. *Magnetic Resonance Imaging* 27(8): 1030–1038.

Sangill R, Wallentin M, Østergaard L, Vestergaard-Poulsen P (2006): The impact of susceptibility gradients on cartesian and spiral EPI for BOLD fMRI. *Magnetic Resonance Materials in Physics, Biology and Medicine* 19(3): 105–114.

Schenck JF (1996): The role of magnetic susceptibility in magnetic resonance imaging: MRI magnetic compatibility of the first and second kinds. *Medical Physics* 23(6): 815–850.

Schneiders NJ (1988): Solutions of two paramagnetic ions for use in nuclear magnetic resonance phantoms. *Medical Physics* 15(1): 12–16.

Schroeter ML, Kupka T, Mildner T, Uludağ K, von Cramon DY (2006): Investigating the post-stimulus undershoot of the BOLD signal—a simultaneous fMRI and fNIRS study. *NeuroImage* 30(2): 349–358.

Scott GC, Joy MLG, Armstrong RL, Henkelman RM (1991): Measurement of nonuniform current density by magnetic resonance. *IEEE Transactions on Medical Imaging* 10(3): 362–374.

Seifritz E, Esposito F, Hennel F, Mustovic H, Neuhoff JG, Bilecen D, Tedeschi G, Scheffler K, Di Salle F (2002): Spatiotemporal pattern of neural processing in the human auditory cortex. *Science* 297(5587): 1706–1708.

Shmueli K, Thomas DL, Ordidge RJ (2007): Design, construction and evaluation of an anthropomorphic head phantom with realistic susceptibility artifacts. *Journal of Magnetic Resonance Imaging* 26(1): 202–207.

Silva AC, Lee S-P, Iadecola C, Kim S-G (2000): Early temporal characteristics of cerebral blood flow and deoxyhemoglobin changes during somatosensory stimulation. *Journal of Cerebral Blood Flow & Metabolism* 20(1): 201–206.

Song AW, Wong EC, Tan SG, Hyde JS (1996): Diffusion weighted fMRI at 1.5 T. *Magnetic Resonance in Medicine* 35(2): 155–158.

Spees WM, Yablonskiy DA, Oswood MC, Ackerman JJH (2001): Water proton MR properties of human blood at 1.5 Tesla: Magnetic susceptibility, T_1, T_2, T^*_2, and non-Lorentzian signal behavior. *Magnetic Resonance in Medicine* 45(4): 533–542.

Stanisz GJ, Odrobina EE, Pun J, Escaravage M, Graham SJ, Bronskill MJ, Henkelman RM (2005): T_1, T_2 relaxation and magnetization transfer in tissue at 3T. *Magnetic Resonance in Medicine* 54(3): 507–512.

Tang L, Avison MJ, Gatenby JC, Gore JC (2008): Failure to direct detect magnetic field dephasing corresponding to ERP generation. *Magnetic Resonance Imaging* 26(4): 484–489.

Tang L, Avison MJ, Gore JC (2009): Nonlinear blood oxygen level-dependent responses for transient activations and deactivations in V1 — insights into the hemodynamic response function with the balloon model. *Magnetic Resonance Imaging* 27(4): 449–459.

Thomas IM, Ma YP, Tan S, Wikswo JP, Jr (1993): Spatial resolution and sensitivity of magnetic susceptibility imaging. *IEEE Transactions on Applied Superconductivity* 3(1): 1937–1940.

Thulborn KR, Waterton JC, Matthews PM, Radda GK (1982): Oxygenation dependence of the transverse relaxation time of water protons in whole blood at high field. *Biochimica et Biophysica Acta (BBA) - General Subjects* 714(2): 265–270.

Truong T-K, Song AW (2008): Single-shot dual-z-shimmed sensitivity-encoded spiral-in/out imaging for functional MRI with reduced susceptibility artifacts. *Magnetic Resonance in Medicine* 59(1): 221–227.

Vanzetta I, Grinvald A (2001): Evidence and lack of evidence for the initial dip in the anesthetized rat: implications for human functional brain imaging. *NeuroImage* 13(6): 959–967.

Vernickel P, Schulz V, Weiss S, Gleich B (2005): A safe transmission line for MRI. *IEEE Transactions on Biomedical Engineering* 52(6): 1094–1102.

Wansapura JP, Holland SK, Dunn RS, Ball WSJ (1999): NMR relaxation times in the human brain at 3.0 tesla. *Journal of Magnetic Resonance Imaging* 9(4): 531–538.

Ward HA, Riederer SJ, Jack Jr. CR (2002): Real-time autoshimming for echo planar timecourse imaging. *Magnetic Resonance in Medicine* 48(5): 771–780.

Weisskoff RM (1996): Simple measurement of scanner stability for functional NMR imaging of activation in the brain. *Magnetic Resonance in Medicine* 36(4): 643–645.

Wong EC, Buxton RB, Frank LR (1998): Quantitative imaging of perfusion using a single subtraction (QUIPSS and QUIPSS II). *Magnetic Resonance in Medicine* 39(5): 702–708.

Yacoub E, Hu X (1999): Detection of the early negative response in fMRI at 1.5 Tesla. *Magnetic Resonance in Medicine* 41(6): 1088–1092.

Yacoub E, Hu X (2001): Detection of the early decrease in fMRI signal in the motor area. *Magnetic Resonance in Medicine* 45(2): 184–190.

Yacoub E, Le TH, Ugurbil K, Hu X (1999): Further evaluation of the initial negative response in functional magnetic resonance imaging. *Magnetic Resonance in Medicine* 41(3): 436–441.

Yacoub E, Shmuel A, Pfeuffer J, Van De Moortele P-F, Adriany G, Ugurbil K, Hu X (2001): Investigation of the initial dip in fMRI at 7 Tesla. *NMR in Biomedicine* 14(7-8): 408–412.

Yacoub E, Vaughn T, Adriany G, Andersen P, Merkle H, Ugurbil K, Hu X (2000): Observation of the initial "dip" in fMRI signal in human visual cortex at 7 tesla. *Proceedings of the International Society for Magnetic Resonance in Medicine* 8: p. 991.

Yang QX, Wang J, Collins CM, Smith MB, Zhang X, Ugurbil K, Chen W (2004): Phantom design method for high-field MRI human systems. *Magnetic Resonance in Medicine* 52(5): 1016–1020.

Yeşilyurt B, Uğurbil K, Uludağ K (2008): Dynamics and nonlinearities of the BOLD response at very short stimulus durations. *Magnetic Resonance Imaging* 26(7): 853–862.

Zaitsev M, Zilles K, Shah NJ (2001): Shared *k*-space echo planar imaging with keyhole. *Magnetic Resonance in Medicine* 45(1): 109–117.

Zandbelt BB, Gladwin TE, Raemaekers M, van Buuren M, Neggers SF, Kahn RS, Ramsey NF, Vink M (2008): Within-subject variation in BOLD-fMRI signal changes across repeated measurements: quantification and implications for sample size. *NeuroImage* 42(1): 196–206.

Zhao Q, Duensing G, Fitzsimmons J (2003): Development of smart phantom for characterizing fMRI informatics tools. *Proceedings of the International Society for Magnetic Resonance in Medicine* 11: p. 1834.